AD-A175 174 DEVELOPMENT OF TECHNIQUES FOR THE USE OF DMSP (DEFENSE METEOROLOGY SATELL.. (U) PHYSICAL DYNAMICS INC BELLEVUE WA J A SECAN 01 JUL 84 PD-NW-84-314R AFGL-TR-84-0167 1/1

UNCLASSIFIED F19628-83-C-0106 F/G 4/1 NL

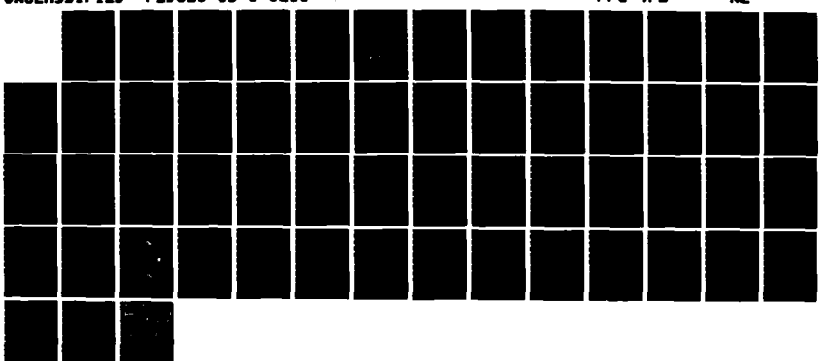

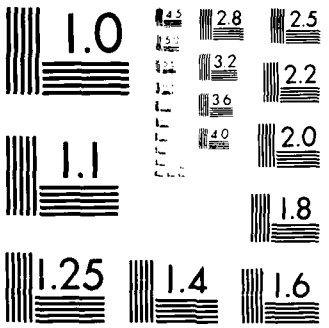

(12)

AFGL-TR-84-0167

DEVELOPMENT OF TECHNIQUES FOR THE USE OF DMSP SSIE DATA IN THE AWS 4D IONOSPHERE MODEL

James A. Secan
Physical Dynamics, Inc.
Northwest Office
P.O. Box 3027
Bellevue, WA 98009

1 July 1984

Scientific Report No. 1

Approved for public release; distribution unlimited.

Prepared for:

AIR FORCE GEOPHYSICS LABORATORY
AIR FORCE SYSTEMS COMMAND
UNITED STATES AIR FORCE
HANSCOM AFB, MASSACHUSETTS 01731

"This technical report has been reviewed and is approved for publication"

SUSAN C. BREDESEN
Contract Manager

WILLIAM J. BURKE
Branch Chief

FOR THE COMMANDER

RITA C. SAGALYN
Division Director

This report has been reviewed by the ESD Public Affairs Office (PA) and is releasable to the National Technical Information Service (NTIS).

Qualified requestors may obtain additional copies from the Defense Technical Information Center. All others should apply to the National Technical Information Service.

If your address has changed, or if you wish to be removed from the mailing list, of if the addressee is no longer employed by your organization, please notify AFGl/DAA, Hanscom AFB, MA 01731. This will assist us in maintaining a current mailing list.

UNCLASSIFIED

SECURITY CLASSIFICATION OF THIS PAGE (When Data Entered)

REPORT DOCUMENTATION PAGE		READ INSTRUCTIONS BEFORE COMPLETING FORM
1. REPORT NUMBER AFGL-TR-84-0167	2. GOVT ACCESSION NO.	3. RECIPIENT'S CATALOG NUMBER
4. TITLE (and Subtitle) DEVELOPMENT OF TECHNIQUES FOR THE USE OF DMSP SSIE DATA IN THE AWS 4D IONOSPHERE MODEL		5. TYPE OF REPORT & PERIOD COVERED Scientific Report No. 1 6. PERFORMING ORG. REPORT NUMBER PD-NW-84-314R
7. AUTHOR(s) James A. Secan		8. CONTRACT OR GRANT NUMBER(s) F19628-83-C-0106
9. PERFORMING ORGANIZATION NAME AND ADDRESS Physical Dynamics, Inc. Northwest Division P.O. Box 3027 Bellevue, WA 98009		10. PROGRAM ELEMENT, PROJECT, TASK AREA & WORK UNIT NUMBERS 61102F 2311G2FF
11. CONTROLLING OFFICE NAME AND ADDRESS Air Force Geophysics Laboratory Hanscom AFB, Massachusetts 01731 Monitor/Susan Bredesen/PHG		12. REPORT DATE 1 July 1984 13. NUMBER OF PAGES 54
14. MONITORING AGENCY NAME & ADDRESS(if different from Controlling Office)		15. SECURITY CLASS. (of this report) UNCLASSIFIED 15a. DECLASSIFICATION/DOWNGRADING SCHEDULE

16. DISTRIBUTION STATEMENT (of this Report)

APPROVED FOR PUBLIC RELEASE; DISTRIBUTION UNLIMITED

17. DISTRIBUTION STATEMENT (of the abstract entered in Block 20, if different from Report)

18. SUPPLEMENTARY NOTES

19. KEY WORDS (Continue on reverse side if necessary and identify by block number)

Ionosphere
Ionospheric modeling
Ionospheric analysis
Defense Meteorology Satellite Program (DMSP)
Topside ionosphere
Total Electron Content (TEC)

20. ABSTRACT (Continue on reverse side if necessary and identify by block number)

Techniques for improved use of topside ionosphere observations within the Air Weather Service (AWS) 4D ionosphere model system are investigated. Topside observations are available at the Air Force Global Weather Central (AFGWC) from the Topside Ionospheric Plasma Monitor (SSIE) on the Block 5D DMSP satellites. The investigations cover three study areas: 1) improvements to the topside ionospheric electron density profile model used within the 4D model, 2) improvements to the ionospheric data preprocessors in the 4D model system, and 3) improvements to the 4D model. Results are presented for tasks completed and in

DD FORM 1 JAN 73 1473 EDITION OF 1 NOV 65 IS OBSOLETE

Unclassified

SECURITY CLASSIFICATION OF THIS PAGE (When Data Entered)

Block 20 (continued)

progress. An evaluation of the topside parametrization used within the International Reference Ionosphere showed it inappropriate for use in the 4D model. This led to initial development of an alternative topside parametrization based on the O^+ to H^+ transition height. The current SSIE N_e(840) data preprocessor (program SSIELD) was evaluated and found to be deficient in several areas, so work was begun on developing improvements for this program. Improvements developed for the 4D model included definition of procedures to configure the model for a full global analysis and the development of procedures to construct 4D model height functions from sets of model electron density profiles.

PREFACE

This report describes the work completed during the first year of a three-year study of ways to enhance the use of data from the USAF Defense Meteorology Satellite Program Topside Ionospheric Plasma Monitor (SSIE) at the Air Force Global Weather Central (AFGWC). This project is a continuation of work completed under contract to Boston College (Boston College Subcontract No. 930-1 to Air Force Geophysics Laboratory Contract F19628-82-K-0011)[1]. Certain results from this project were included as part of the program documentation written for the Air Weather Service 4D Ionospheric Analysis Model provided under Defense Nuclear Agency contract DNA001-83-C-0097. I wish to acknowledge the assistance of Dr. Fred Rich, AFGL/PHG, and Mr. Bob Bussey, AFGWC/TSIS, during this project year.

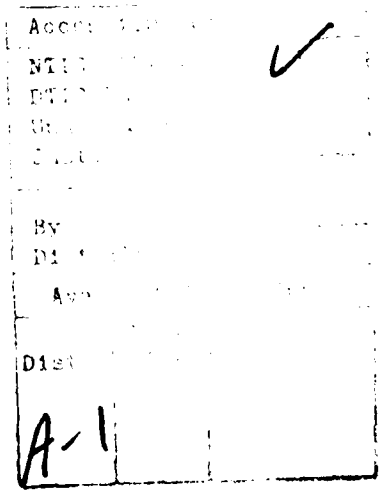

CONTENTS

LIST OF FIGURES

1. INTRODUCTION

Defense Meteorology Satellite Program (DMSP) Block 5D satellites have included Topside Ionospheric Plasma Monitor (SSIE) sensors since mid 1977[3,4]. Ionospheric electron density, $N_e(840)$, and plasma scale height, $H_p(840)$, at the satellite altitude, nominally 840 km, from the SSIE sensors are routinely processed at the Air Force Global Weather Center (AFGWC) for specification of the state of the earth's ionosphere. Figure 1 is a simplified flow diagram of data from the SSIE sensors within AFGWC. SSIE data are stripped from the DMSP satellite telemetry stream and written to a temporary file (IEPREPFILE) by the AFGWC DMSP processing system. Program SSIE reads the raw SSIE data from this file, calculates electron densities and plasma scale heights[3,4], and writes out a data record for every 64 seconds containing an average $N_e(840)$ value and $H_p(840)$ value to a temporary file (IFLUXFILE). Program LDIPIE reads the data records from this file, reformats them, and writes them into the Astrogeophysical Data Base (AGDB)[5]. Program SSIELD reads SSIE $N_e(840)$ data for the most recent 24 hours from the AGDB, constructs 10° latitude by 15° longitude northern-hemisphere grids of $N_e(840)$ for each of the 24 hours, and writes them to a gridded-data file (FOURDGRIDS)[6]. These data are merged with data grids from the f_oF2 and TEC preprocessors and written to temporary file 18 by program GRDOUT as observation data sets[2]. The Air Weather Service (AWS) 4D Ionospheric Analysis Model[7,8] inputs the observation data sets from temporary file 18 and produces a consistent analysis of the ionospheric electron density distribution over the entire northern hemisphere.

The primary objective of this project is to study methods for improving the use of the SSIE $N_e(840)$ and $H_p(840)$ data by the 4D model system, identified in Figure 1 by those files and programs within the dashed box. The studies have focused on possible improvements to the 4D model, particularly to its internal electron-density profile model, and to the various 4D model system preprocessors.

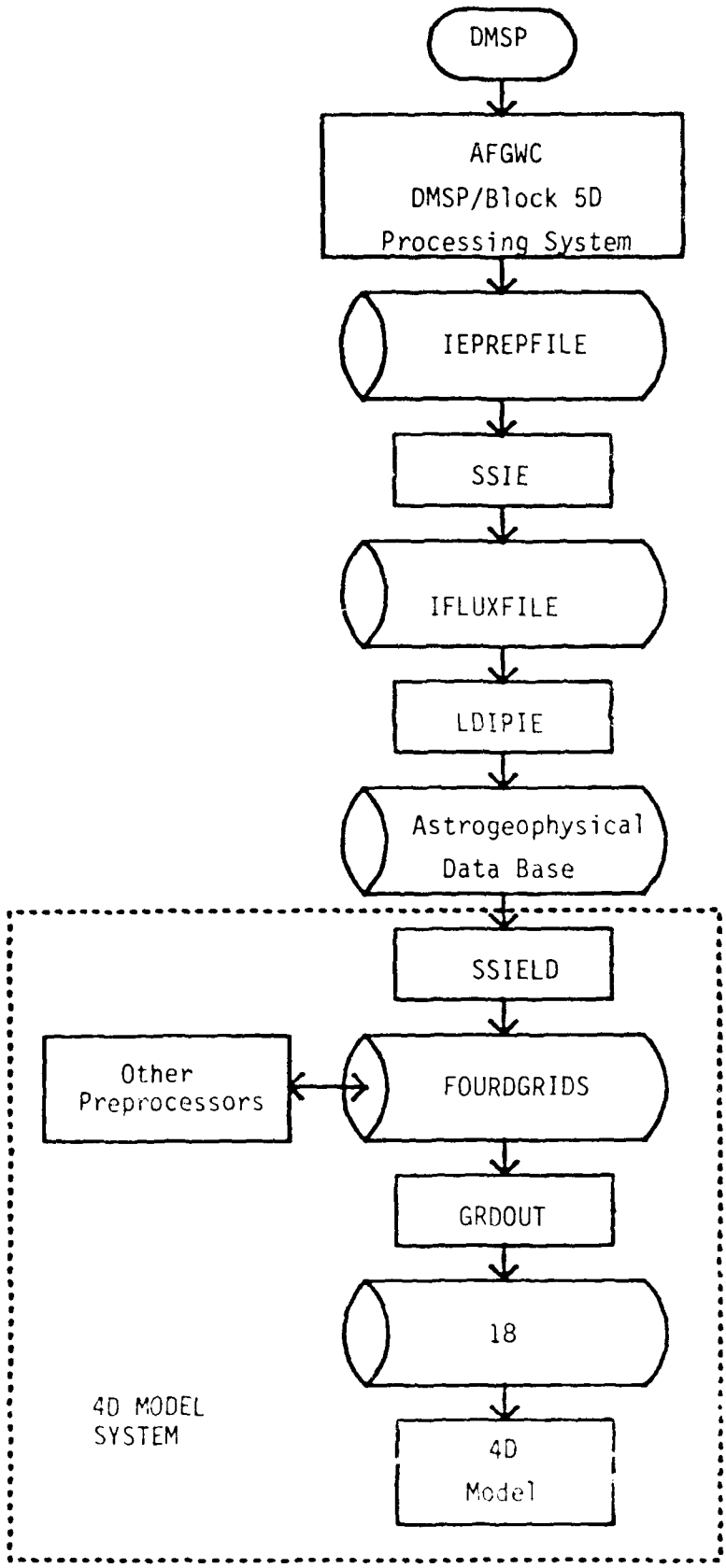

Data Format

Telemetry stream

SSIE telemetry data

$N_e(840)$ averages, $H_p(840)$

Data-type 18 records

$N_e(840)$ grids

Observation data sets

Figure 1. SSIE data processing flow at AFGWC.

2. PROJECT DEFINITION

The first step in the project was to define specific tasks to pursue within the areas of research defined in the project proposal and statement of work. This study resulted in the following list of tasks to be completed during the project:

1. Determine the modifications required to configure the 4D ionospheric analysis model for a full global analysis.

2. Investigate the use of the profile parametrization used in the IRI79 reference ionosphere[9] as a replacement for the Damon-Hartranft parametrization currently used in the 4D model.

3. Derive sets of height-profile basis functions for the 4D model using plasma frequency profiles from the IRI79 reference ionosphere.

4. Investigate techniques for improving the preparation of data grids of $N_e(840)$ from the SSIE $N_e(840)$ observations.

5. Work with personnel from AFGL and AFGWC to develop improved techniques for combining TEC and SSIE $N_e(840)$ data into a single specification of the topside ionosphere.

6. Investigate alternative parametrizations of the topside ionosphere which would use the full set of data available from the SSIE sensors and all other available data, including Total Electron Content (TEC) data, to specify the electron density profile above the F2-layer peak.

7. Begin an investigation into ways to use data from the SSIE sensors, in conjunction with other observations, for modeling the ionospheric subauroral trough as part of the 4D model preprocessor system.

Tasks 1, 2, and 3 have been completed, and work has begun on Tasks 4, 5, and 6. These tasks fall generally into three main studies: 1) Topside Profile Model Study (Tasks 2 and 6), 2) Ionospheric Data Preprocessor Improvements Study (Tasks 4, 5, and 7), and 3) 4D Model Improvements Study (Tasks 1 and 3). Work completed this project year will be presented separately for each of these three study areas.

3. TOPSIDE PROFILE MODEL STUDY

This study includes Tasks 2 and 4 of the project. The overall objective of this study is to investigate improved parametrizations of the topside ionospheric electron density profile for use within the 4D model.

3.1 Task 2: IRI79 Topside Parametrization

The 4D uses a model of the electron density profile in the topside ionosphere to interpolate between observed values of f_oF2 and h_mF2 and *in-situ* observations of $N_e(h)$ and $H_p(h)$, the electron density and plasma (pressure) scale height, at DMSP altitudes. The profile model must, therefore, be designed such that its parameters can be easily adjusted to fit the input data and behave reasonably from h_mF2 to 2000 km. In this context, reasonable behavior is defined as follows:

(1) The electron density scale height, defined as

$$H_n(h) = - \left[\frac{d}{dh} \ln N_e(h) \right]^{-1} , \qquad (1)$$

is positive throughout the topside.

(2) There are no sharp discontinuities in either $N_e(h)$ or $H_n(h)$ (important for ray traceing applications).

(3) The scale height, $H_n(h)$, varies smoothly from ∞ at h_mF2 through the value calculated at the DMSP altitude (nominally 840 km) to values at 2000 km consistent with the expected temperature and mean ionic mass at that altitude.

Currently, the 4D model uses the modified Damon-Hartranft model[10,11], denoted the DHR model (also referred to as the RBTEC model), to interpolate in the topside. The two major problems with this model, in this application, are: 1) the profile assumes that the only ionic constituent at all altitudes is O^+, and 2) only three of the four data values to be input (f_oF2, M3000, $N_e(840)$, and $H_n(840)$) can be fit at one time. An interim solution to the second problem was developed during earlier work on this project[2], but the resulting profiles can sometimes exhibit unreasonable behavior in $H_n(h)$.

The major thrust of Task 2 was to investigate the IRI79 model to determine if 1) the IRI79 topside parametrization could be modified for use within the 4D model, and 2) the profile shape provided by the IRI79 model is sufficiently better than the DHR model to justify replacement of the DHR model by the IRI79 model in the 4D.

The first step of this task was to modify the IRI79 topside profile parametrization to allow the profile to be fit to input topside observations of $N_e(h)$ and $H_n(h)$. The IRI79 model uses an exponential function for the topside $N_e(h)$ profile of the form[9]

$$N_e(h) = N_m F2 \; e^{-Y(h)} \tag{2}$$

where

$$Y(h) = R \left[\beta \eta E_1(h, 394.5, \beta) + 100 \, \zeta E_1(h, 300, 100) \right] - (h - h_m F2) \, \zeta \tag{3}$$

$$R = \left(\frac{1000 - h_m F2}{700} \right),$$

$$E_1(h,a,b) = \ln \left| \frac{1 + \exp\left(\frac{X(h)-a}{b} \right)}{1 + \exp\left(\frac{X(h_m F2)-a}{b} \right)} \right|$$

$$X(h) = \frac{(h - h_m F2)}{R} + 300 - \delta,$$

and β, η, ζ, and δ are functions of various geophysical parameters. The scale height, defined as in Equation 1, can be calculated from Equations 2 and 3 to give

$$H_n(h)^{-1} = \eta E_2(h,394.5,\beta) + \zeta\left[E_2(h,300,100) - 1\right] \quad (4)$$

where

$$E_2(h,a,b) = R\frac{d}{dh}E_1(h,a,b) = \frac{1}{1+\exp -\left[\left(\frac{X(h)-a}{b}\right)\right]} \quad .$$

An iterative technique was developed to fit this profile to input values of f_oF2, h_mF2, $N_e(840)$, and $H_n(840)$ by adjusting the two parameters, η and ζ, through

$$\eta' = \left[\left\{\left[E_2(h,\ 394.5,\ \beta) + \frac{\zeta}{\eta}\ E_2(h,300,100)-1\right]\right\}H_n(840)\right]^{-1} \quad (5)$$

and

$$\beta' = -\left[\frac{\frac{Y(840)}{R} - \beta\eta' E_1(h,394.5,\beta)}{\frac{(h-h_mF2)}{R} - 100E_1(h,300,100)}\right] \quad (6)$$

where

$$Y(840) = \ln\left|\frac{N_e(840)}{N_mF2}\right| \quad .$$

This technique was successful in calculating a profile which reproduced the input data, but the resulting profiles were quite often unreasonable away from the data points, at times producing secondary peaks in $N_e(h)$ just above the F2 peak. A second technique was then developed in which the parameter, β, was adjusted through

$$\beta' = \frac{\left[Y(840)+(h-h_mF2)\zeta\right]\frac{1}{R} - 100\ E_1(h,300,100)}{\eta' E_1(h,394.5,\beta)} \quad , \quad (7)$$

replacing Equation 6, but this technique worked no better than the first. A study of the IRI79 topside was then begun to determine the source of the difficulties in producing reasonable profile behavior using the IRI79 topside parametrization.

Since the desire for a more realistic topside profile shape was the primary reason a replacement for the DHR model was being sought, the study focused on the scale height profiles produced by Equation 4. The $H_n(h)$ profiles thus calculated were compared with the results of an analysis of $H_n(h)$ profiles taken from Alouette topside soundings[12]. Figure 2 shows a representative sample of daytime, midlatitude (dip latitude ~45°), solar

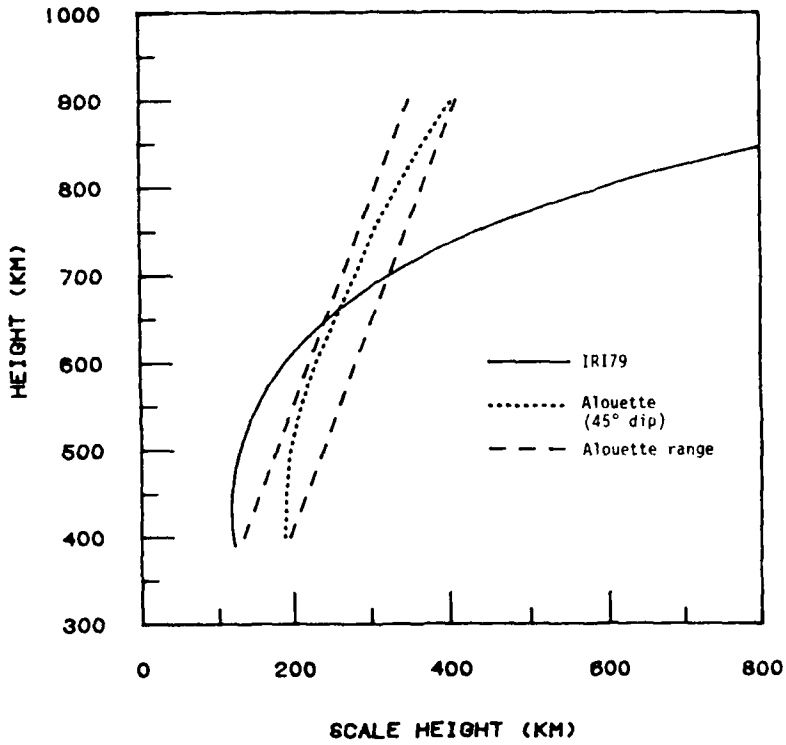

Figure 2. Comparison of IRI79 and Alouette daytime, midlatitude scale heights.

minimum $H_n(h)$ profiles from the IRI79 model (solid curve) and from Alouette soundings (dotted curve is a single representative $H_n(h)$ profile; the dashed curves bracket all $H_n(h)$ profiles for the Alouette pass from which the individual profile was taken). The pattern of IRI79 $H_n(h)$ profile departures from Alouette soundings shown in Figure 2, scale heights roughly 30

to 40% too low just above the F2 peak and up to 300% too high at 900 km, was typical for all daytime comparisons. Figure 3 shows a plot of scale heights at various altitudes as a function of dip latitude for summer day and summer night. The plot for daytime shows the persistence of the pattern displayed in Figure 2. The night plot shows that although the IRI79 scale heights are not too bad at lower midlatitude night, the model departures revert to their daytime pattern within the transition into the light-ion trough.

A final comparison was made between TEC values calculated by both the IRI79 and DHR models and observed TEC from the USAF Sagamore Hill Observatory. The model profiles were calculated using ITS-78 model[13] values for f_0F2 and M3000 modified by adding the difference between observed and ITS-78 values at Wallops Island, which is near the Sagamore Hill ionospheric penetration point. Two sets of data were used, the first taken from monthly median data used in evaluation of the Damon-Hartranft model[10] from solar cycle 20, and five-day mean values from AFGWC from solar cycle 21. Table 1 shows the results of this comparison. In all cases the DHR model was appreciably closer to the observed TEC than the IRI79 model. While not as extensive a comparison as that made by McNamara and Wilkinson[14], the data used are fairly representative of median midlatitude behavior and favored neither model *a priori*.

TABLE 1. Comparison of observed and model TEC (DHR and IRI79).

Date	SSN	UT	LT	Total Electron Content ($\times 10^{16}$ el/m^2) Observed	DHR Model	IRI79 Model
Jan 1968	122	0500	0020	6.6	7.2 (+11%)	13.7 (+108%)
Jan 1968	122	2000	1520	41.0	37.8 (- 8%)	57.6 (+ 40%)
Mar 1968	92	1100	0620	6.4	8.3 (+28%)	12.7 (+ 95%)
Mar 1968	92	1600	1120	33.0	34.1 (+ 3%)	44.5 (+ 35%)
Jul 1969	96	0400	2320	12.0	14.5 (+21%)	19.8 (+ 65%)
Jul 1968	96	1800	1320	18.0	17.8 (- 1%)	21.4 (+ 19%)
Sep 1968	117	0100	2020	14.0	17.2 (+23%)	28.1 (+101%)
Sep 1968	117	1500	1020	24.0	24.0 (0%)	39.6 (+ 65%)
Sep 1983	86	0000	1920	17.5	19.7 (+13%)	25.4 (+ 45%)
Sep 1983	86	0600	0120	6.4	5.6 (-13%)	9.5 (+ 48%)
Sep 1983	86	1200	0720	11.0	11.8 (+ 7%)	17.7 (+ 61%)
Sep 1983	86	1800	1320	17.2	17.6 (+ 2%)	21.5 (+ 25%)

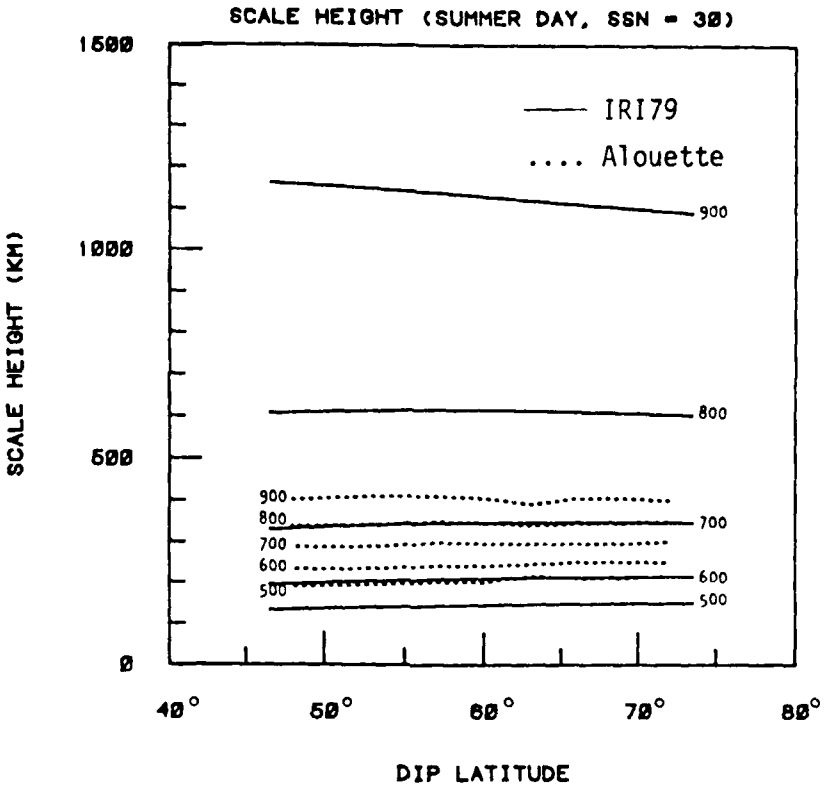

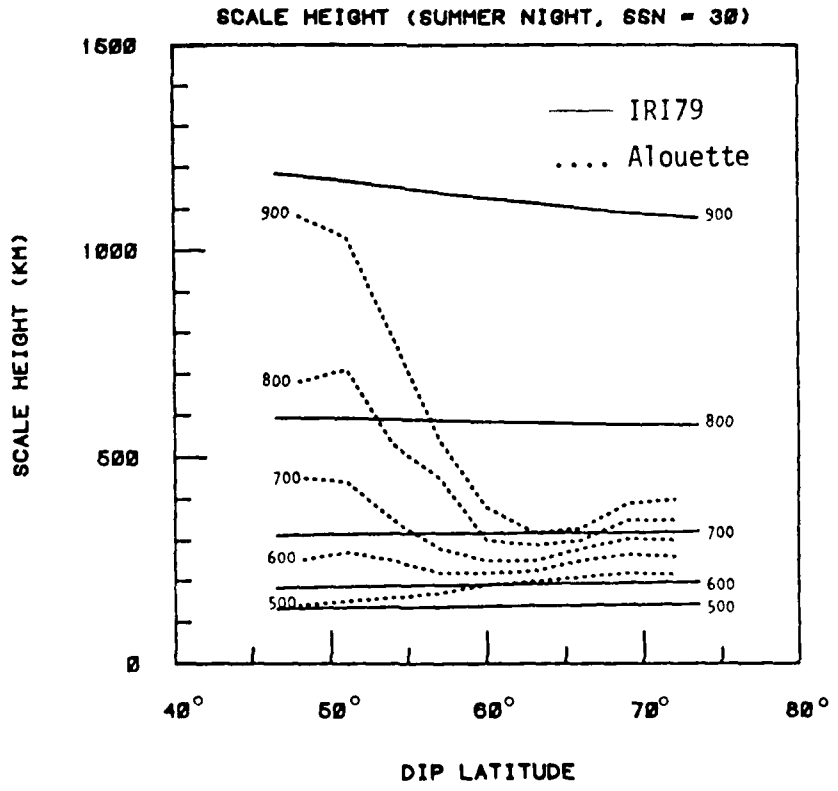

Figure 3. Latitudinal variation of $H_n(h)$ from the IRI79 model and from Alouette soundings. Altitude (km) labels are given on the right for IRI79, on the left for Alouette.

In conclusion, it was decided that the IRI79 model, in its current form, is not a viable replacement for the DHR model for the following reasons:

1. Although the topside parametrization used in the IRI79 model could be modified to fit input observations of f_oF2, h_mF2, $N_e(840)$, and $H_n(840)$, the resulting profiles often did not behave reasonably, occasionally producing additional $N_e(h)$ peaks above h_mF2. This was particularly true if the input $N_e(840)$ or $H_n(840)$ differed significantly from that calculated from IRI79 using only f_oF2 and h_mF2 as inputs.

2. The electron density scale height, $H_n(h)$, calculated from the IRI79 model ranges from values which are slightly too small just above the F2 peak to values which are much too large above 800 km, particularly during the day and poleward of the plasmapause at night.

3. The top of the IRI79 model is at 1000 km, and the 4D model requires a profile up to 2000 km. Extending the IRI79 profile calculation above 1000 km results in an electron distribution with an effectively infinite scale height above roughly 1200 km.

4. The sub-auroral light-ion trough, a major feature in the nighttime topside ionosphere, is not present in the IRI79 model.

5. Comparisons of TEC calculated from profiles generated by the two models showed that, at best, the IRI79 model performed slightly better than the DHR model only on occasion, and often did much worse.

3.2 Task 6: Alternative Topside Parametrization

Since the IRI79 model proved unsuitable for this project, work was begun on Task 6, developing a new parametrization for the topside to replace the DHR model. The basic concept that evolved is to develop an empirical topside model which treats the ionosphere profile separately above and below the height where $N(O^+)=N(H^+)$, h_T, and fits the two profiles together smoothly at h_T using a spline fit procedure which produces a smooth transition in both $N_e(h)$ and $H_n(h)$ between profile sections. This requires three separate models: 1) an $N_e(h)$ model for the height region $h_mF2 \leq h < h_T$, 2) an $N_e(h)$ model for $h_T < h \leq 2000$, and 3) a model for the behavior of h_T.

The starting point for the profile model is the following:

1) $h_m F2 \leq h \leq h_T$

$$N_e(h) = N_m F2 \exp\left(1 - z_1 - e^{-z_1}\right)$$

where

$$z_1 = \frac{h - h_m F2}{H_1(h)}$$

$$H_1(h) = H_o(\phi_m, LT) \ln \left| \frac{h}{85.4} \right|$$

ϕ_m : magnetic latitude

LT : local time, and

2) $h_T < h \leq 2000$ KM

$$N_e(h) = N_T e^{-z_2}$$

where

$$z_2 = \frac{h - h_T}{H_2(h)}$$

$$H_2(h) = H_T \exp \left| \frac{h - h_T}{\beta} \right| .$$

The profile in the lower section is the DHR model, which is a reasonable model for a predominantly O^+ ionosphere. The upper profile is an exponential distribution with an exponentially varying scale height with several free parameters, N_T, H_T, and β, which can be adjusted as necessary to fit observations.

A preliminary model has been developed for h_T based on analyses of topside sounder data[14] which allows h_T to vary as a function of magnetic latitude, local time, season, and the 10.7 cm solar flux. Figures 4a and 4b show examples of the results from this preliminary model. The solid lines in

the plots are from the model, and the dashed lines are data taken from Figures 9 and 11 in Titheridge[15] (1976a). Work will continue on this model during the next project year. The solar cycle variation of h_T will be checked against recent observations[16], and the possibility of varying the location of the equatorward edge of the light-ion trough in the h_T model as a function of magnetic activity[17] or from observations will be investigated.

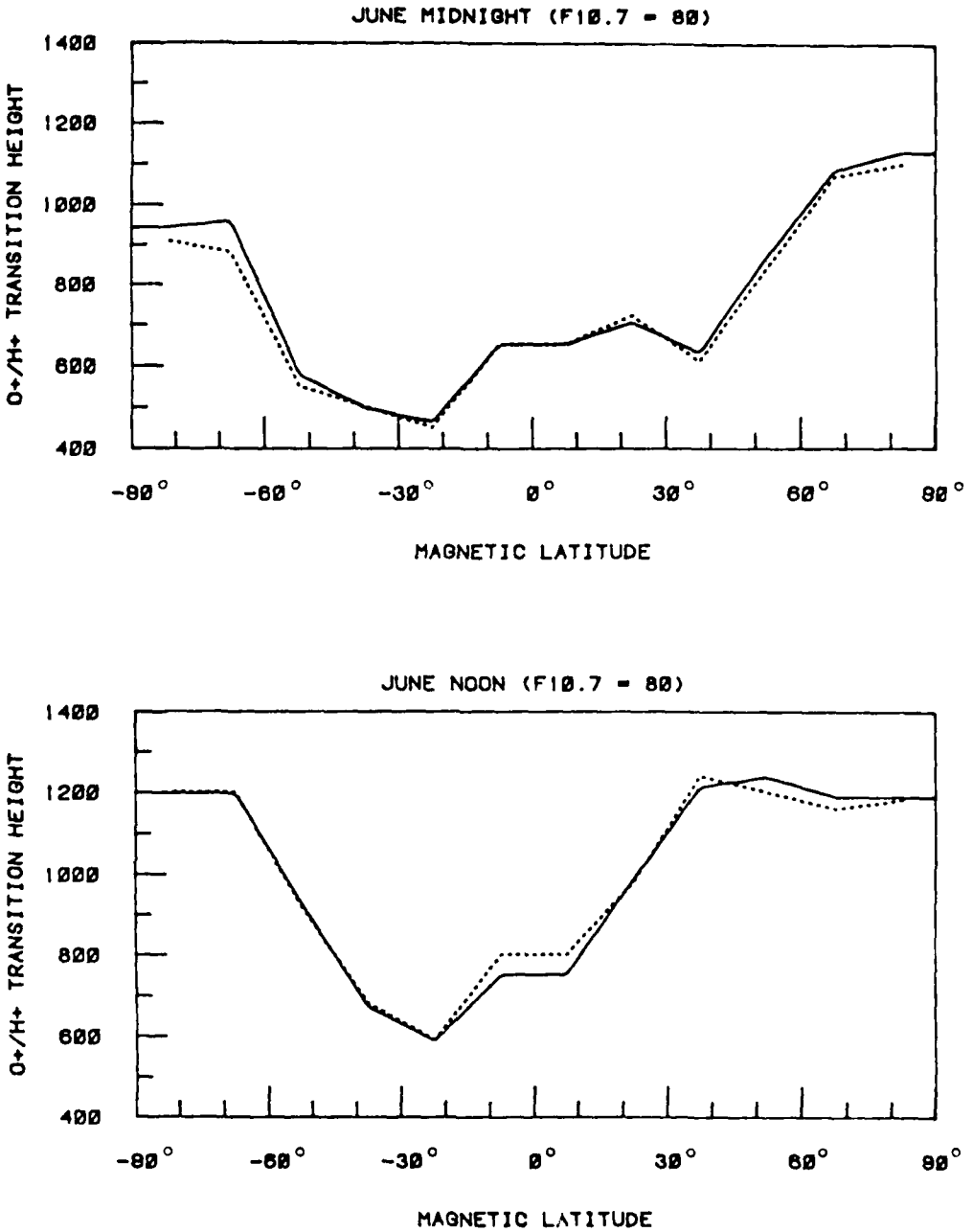

Figure 4a. Latitudinal variation of h_T for local noon and midnight (June). Solid lines are from topside sounder data[15], dotted lines are from the h_T model.

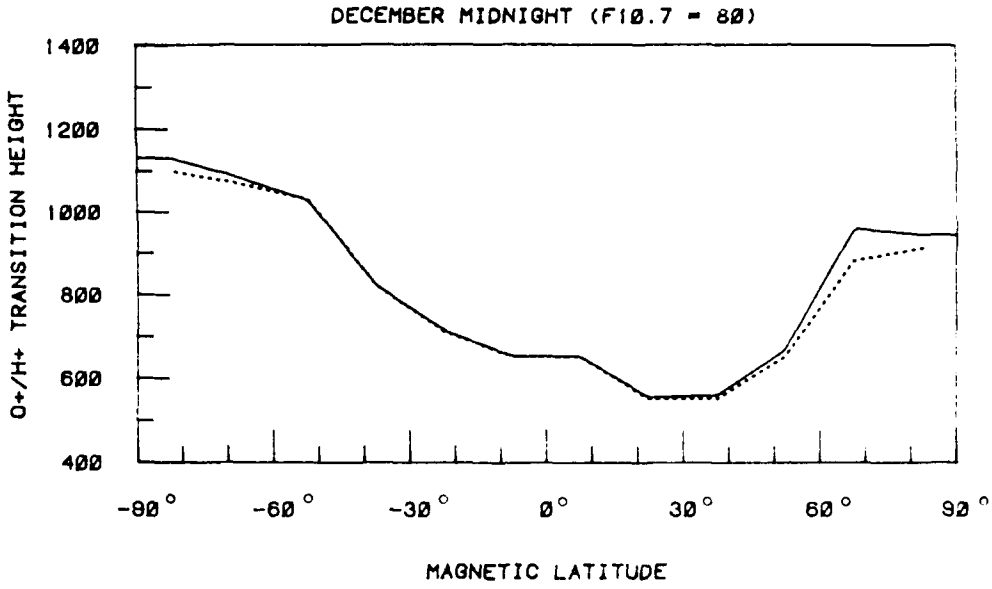

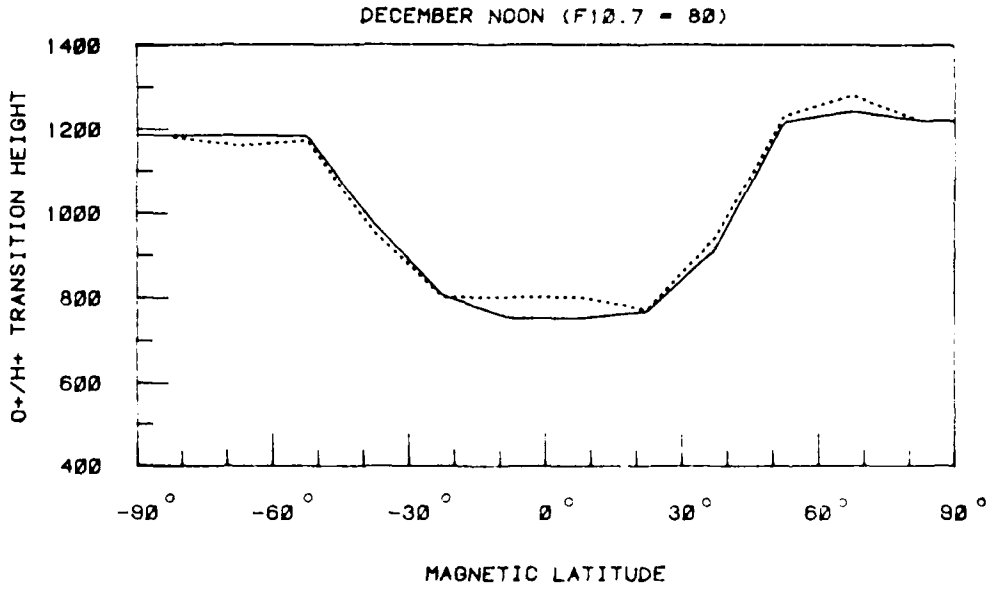

Figure 4b. Latitudinal variation of h_τ for local noon and midnight (December). Solid lines are from topside sounder data[15], dotted lines are from the h_τ model.

4. IONOSPHERIC DATA PREPROCESSORS STUDY

Limited investigations into analysis stability problems with the 4D model led to the development of front-end data preprocessors for f_0F2 and TEC data by AFGWC/TSIS[18,19,20]. These preprocessors use simple curve-fitting techniques to generate equally spaced grids of f_0F2 and TEC values from data available in the Astrogeophysical Data Base (AGDB)[21]. In the contract prior to the current one, a 4D model preprocessor system[2] was designed around these two preprocessors, programs FORIER (f_0F2 data) and POLY1 (TEC data), and a third preprocessor for SSIE $N_e(840)$ data, program SSIELD[6], provided by another contractor.

This system, tested and installed at AFGWC, was to be the starting point for the tasks under this study area. Unfortunately, as of the start of this phase of the project, the SSIELD program was still not operational at AFGWC, and was neither sufficiently tested nor adequately documented to be of any use. Thus, this study area was begun by assisting AFGL/PHG with an assessment of the SSIELD program.

4.1 Program SSIELD Assessment

4.1.1 SSIELD Overview

At the request of AFGL/PHG, tests of the SSIELD program designed to assess the program's status were conducted during a visit to AFGWC in late March, 1984.

The SSIELD program produces equally spaced grids of $N_e(840)$ from SSIE data in the AGDB in a two-phase process[6]. First, 24 hours of SSIE data for a single DMSP satellite are read from the AGDB and are used to construct equally spaced latitude/longitude grids for the ascending- and descending-node local times. If data for a second DMSP satellite are available, this step is repeated for data from the second satellite. Second, the two (or four) local time grids are "spread" to other local times by a weighted interpolation scheme. Output from the program consists of equally spaced latitude/longitude grids for each of 24 UT hours.

The construction of the local time grids, or maps, is accomplished by a method known as "kriging[22]." This method assumes that the spatial stochastic

field described by the data can be described by the sum of a mean, or trend, field and a fluctuation field. After modeling and removing the trend, the fluctuation field is modeled in terms of the covariance function of the process. In SSIELD, the trend is removed by fitting the data for a given local time by a simple polynomial function in latitude and the sine of the longitude[6]. This trend is removed from the data, and the resulting fluctuation field is used to estimate the covariance function, C. In estimating C, two major assumptions are made:

1. The fluctuation field is homogeneous and isotropic. Therefore C is a function only of the separation between points, and not a function of point location or direction.

2. The covariance function is of the form

$$C(d) = \sigma^2 e^{-\beta d} \tag{8}$$

where d is the distance between two points, and σ^2 and β are parameters to estimate from the fluctuation field.

The σ^2 parameter is estimated by the variance in the fluctuation field. The β parameter is estimated by fitting equation 8 to a discrete covariance function estimate calculated from the input data. Should the process of estimating fail, the program uses a default value for β of 0.1. The trend and covariance function estimates are then used to produce equally spaced local time maps.

After all input data have been converted to local time maps, a model of the electron density at 840 km is used to interpolate to other local times. For a given latitude/longitude grid point, the two (four) values from the local time maps, weighted by error estimates, are used to shift the local time variation curve generated from the Bent model for that grid point. This process is repeated for all grid points, and the resulting 24 local time maps are converted to 24 UT maps and written out to file FOURDGRIDS.

The electron density model used in SSIELD is a simple spectral expansion of $N_e(840)$ fields extracted from electron density profiles constructed using the Bent ionosphere model[23]. Four sets of 24 northern hemisphere $N_e(840)$ grids, one grid for each UT hour and one set for each season, were fit with associated Legendre function polynomials of degree 9 and order 2. Interpolation in day-of-year is done with trigonometric functions; no interpolation is done in UT. Although this model represents only a simple snapshot of the Bent model, it will be referred to as the "spectral Bent model" in the remainder of this report.

4.1.2 Assessment Test Description

A series of tests of the SSIELD program was designed to assess the program's current status for AFGL/PHG. Nine tests were planned - eight using $N_e(840)$ data from models as input and one using "live" SSIE data from the AGDB. Four model ionospheres were generated, three using the DHR model[11] (sunspot numbers 10, 60, and 120) and one using the spectral Bent model from SSIELD. A date of 15 June was used for both models, to avoid a negative $N_e(840)$ problem in the spectral Bent model described later. Two tests were generated from each model ionosphere - a single-satellite test with data along a simulated DMSP F6 satellite orbit (nominally dawn-dusk) and a two-satellite case with data along simulated F6 and F7 (nominally 10LT - 22LT) orbits. These eight model tests were to be supplemented by daily SSIELD runs on whatever SSIE data from satellite F7 were available in the AGDB.

Prior to the actual testing, several coding errors were discovered in extracting the spectral Bent model routines from SSIELD, as well as severe problems with several of the model coefficient sets used to represent the Bent $N_e(840)$ values. The coding errors were corrected prior to testing, but correction of the special Bent coefficients were beyond the scope of the assessment. Figures 5 and 6 illustrate this problem with the Bent coefficients. Not only is the latitudinal behavior unrealistic, but the model can produce negative density values at high latitudes during almost half of the year. Since this problem could not be corrected before the assessment testing, all model tests were run using a date of 15 June (day 166) which, as can be seen in Figure 6, should minimize the impact of this problem. It must be kept in mind, however, that the test results will only indicate how well SSIELD performs during the short time of the year that the spectral Bent model is reasonably behaved (roughly 15 June ± two weeks) and will not indicate how poorly it might perform at other times.

4.1.3 Assessment Test Results and Evaluation

Due to untimely degradation of the SSIE sensors on the F7 satellite, no data were available for live testing, so all testing was on bogus data as described in 4.1.2. The overall results of the eight tests are summarized in Table 2.

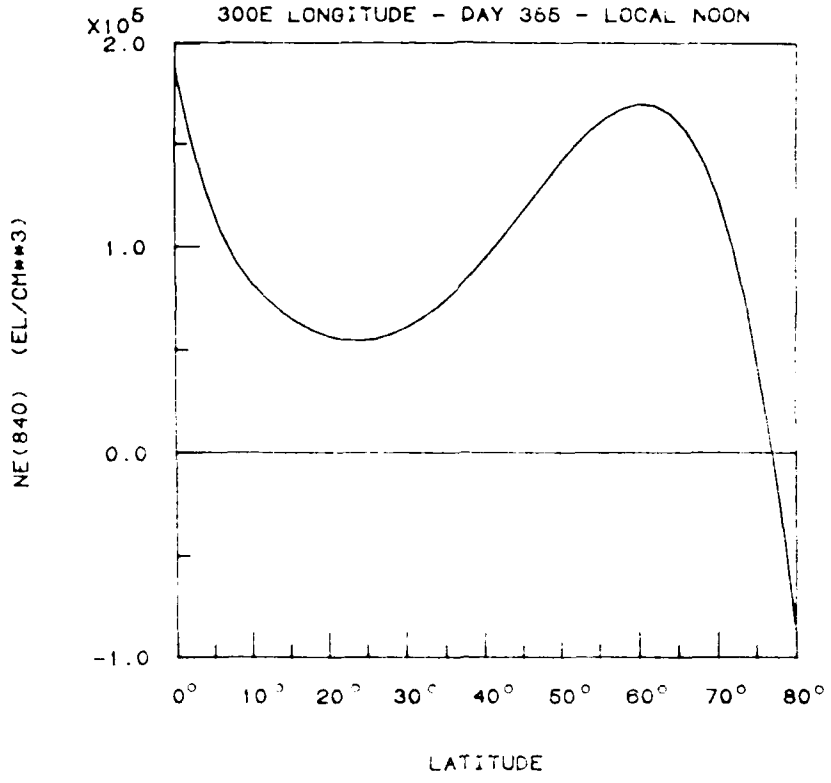

Figure 5. Latitudinal variation of $N_e(840)$ at local noon from the spectral Bent model.

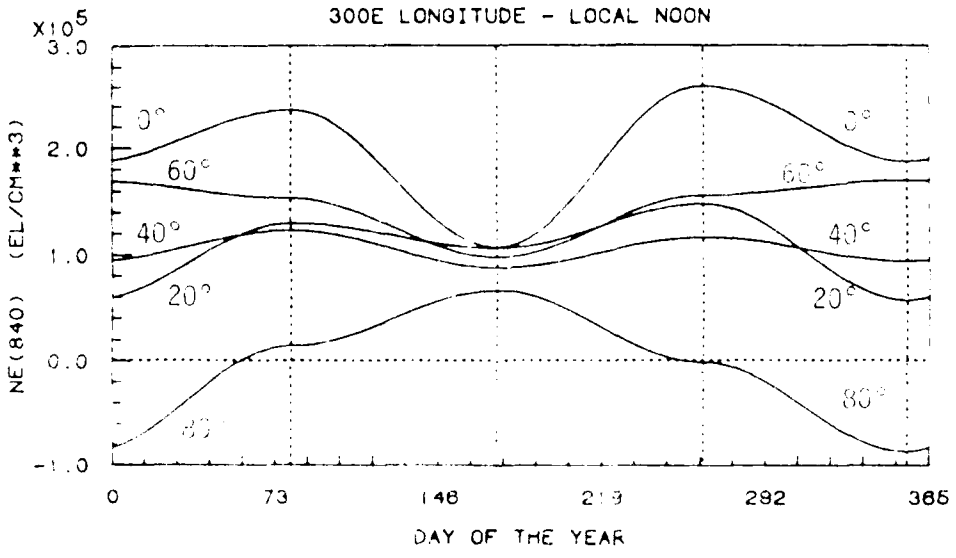

Figure 6. Seasonal variation of $N_e(840)$ at local noon from the spectral Bent model for various latitudes.

TABLE 2. SSIELD Test Analysis Summary.

Input Model	RMS Error	RMS % Error	Beta 0600LT	Beta 1800LT	Beta 000LT	Beta 2200LT
Bent; F6 only	1.06×10^4	22.6	F	0.086	-	-
Bent; F6, F7	1.11×10^4	22.6	F	0.086	0.124	F
DHR(10)*; F6 only	1.45×10^4	105.2	F	0.144	-	-
DHR(10); F6, F7	1.48×10^4	88.1	F	0.144	F	F
DHR(60); F6 only	2.15×10^4	45.2	0.086	F	-	-
DHR(60); F6, F7	2.12×10^4	39.4	0.086	F	F	0.141
DHR(120); F6 only	3.50×10^4	33.7	F	F	-	-
DHR(120); F6, F7	3.37×10^4	31.9	F	F	0.237	0.186

The first two columns for each test case are the total RMS difference and RMS percent difference between the $N_e(840)$ grids output by SSIELD and the grids generated by the various models from which the simulated DMSP data were extracted. The last four columns indicate whether the covariance function determination (subroutine COVEST) was successful for the given LT map. If a value is given, it corresponds to the β variable in the covariance function; an "F" indicates that COVEST failed. Since the analyses for 0600LT and 1800LT are the same for either one- or two-satellite inputs, the β values for these times will be the same in both cases, for a total of 16 independent LT map analyses in the 8 test cases. Of these 16 analyses, the COVEST analysis failed 9 times.

Figure 7 shows a breakdown of the RMS values given in Table 2 as functions of latitude and local time, respectively, for the 4 two-satellite tests. The solid lines in these figures are for the DHR model inputs, the dashed lines are for the spectral Bent model inputs. The problems at 80° latitude are primarily due to inexplicably high $N_e(840)$ values in the SSIELD

*The numbers in parentheses indicate the sunspot number used by the model.

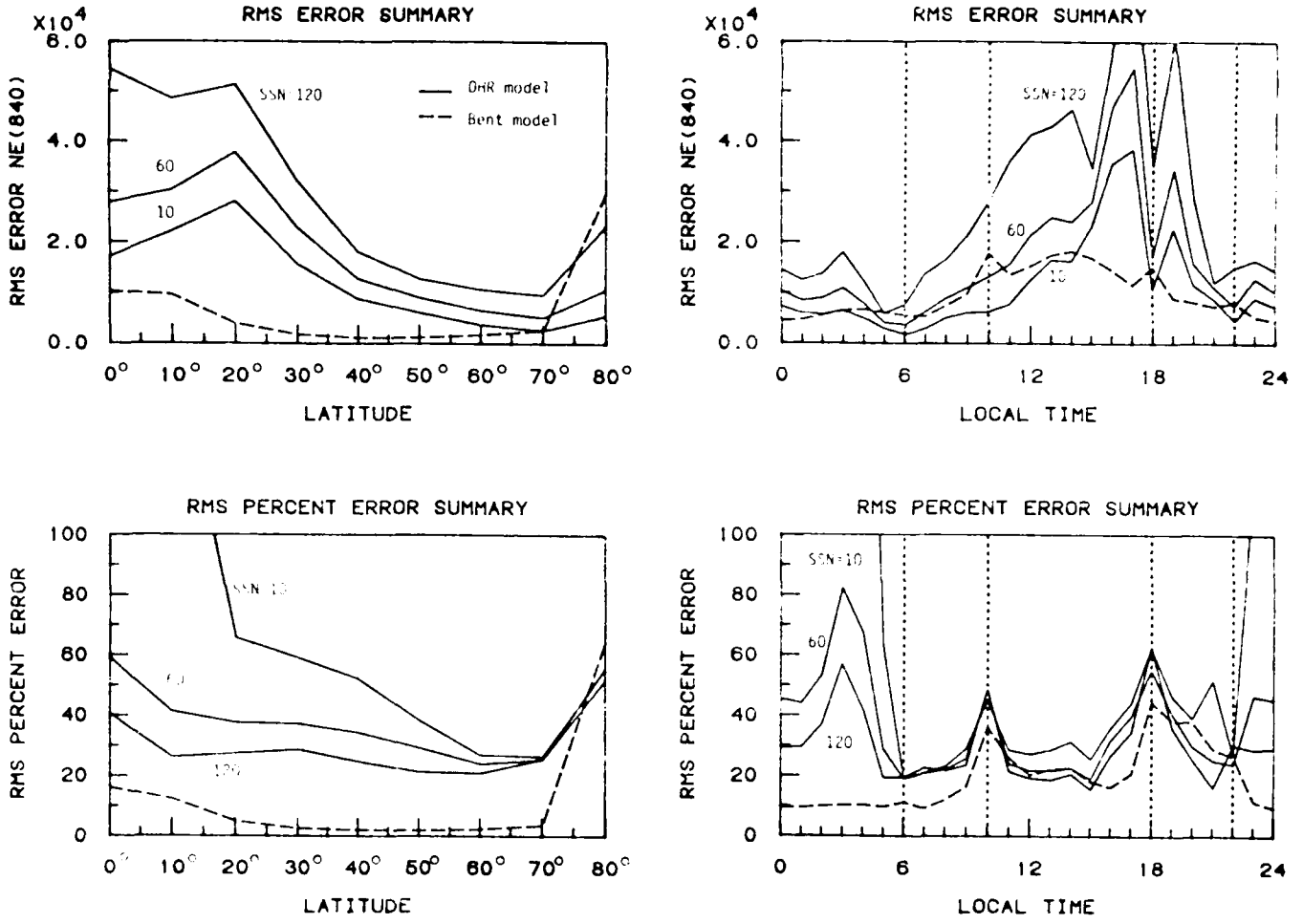

Figure 7. Variation of RMS error and RMS percent error with latitude and with local time for all two-satellite tests.

analysis at 1000LT and 1800LT, but the equatorial increase in RMS percent error occurs at all local times. The local time plots show, rather graphically, definite problems with the LT-spreading algorithm. The vertical dotted lines are at local times where SSIELD constructed LT-maps (0600, 1000, 1800, and 2200LT). The fact that something "happens" in the analysis at these times, particularly at 1800LT, indicates a failure of the LT-spreading process. This can also be seen in Figure 8, which shows the longitudinal variation of $N_e(840)$ for three latitudes from the 00UT map of the DHR(60) two-satellite test. Again, the analysis shows definite discontinuities at the times where LT maps were constructed, indicated on the figure by vertical dotted lines. (Note: The RMS error summary plot in Figure 8 does not show a dip at 1000LT due to purely coincidental balancing of smaller errors at

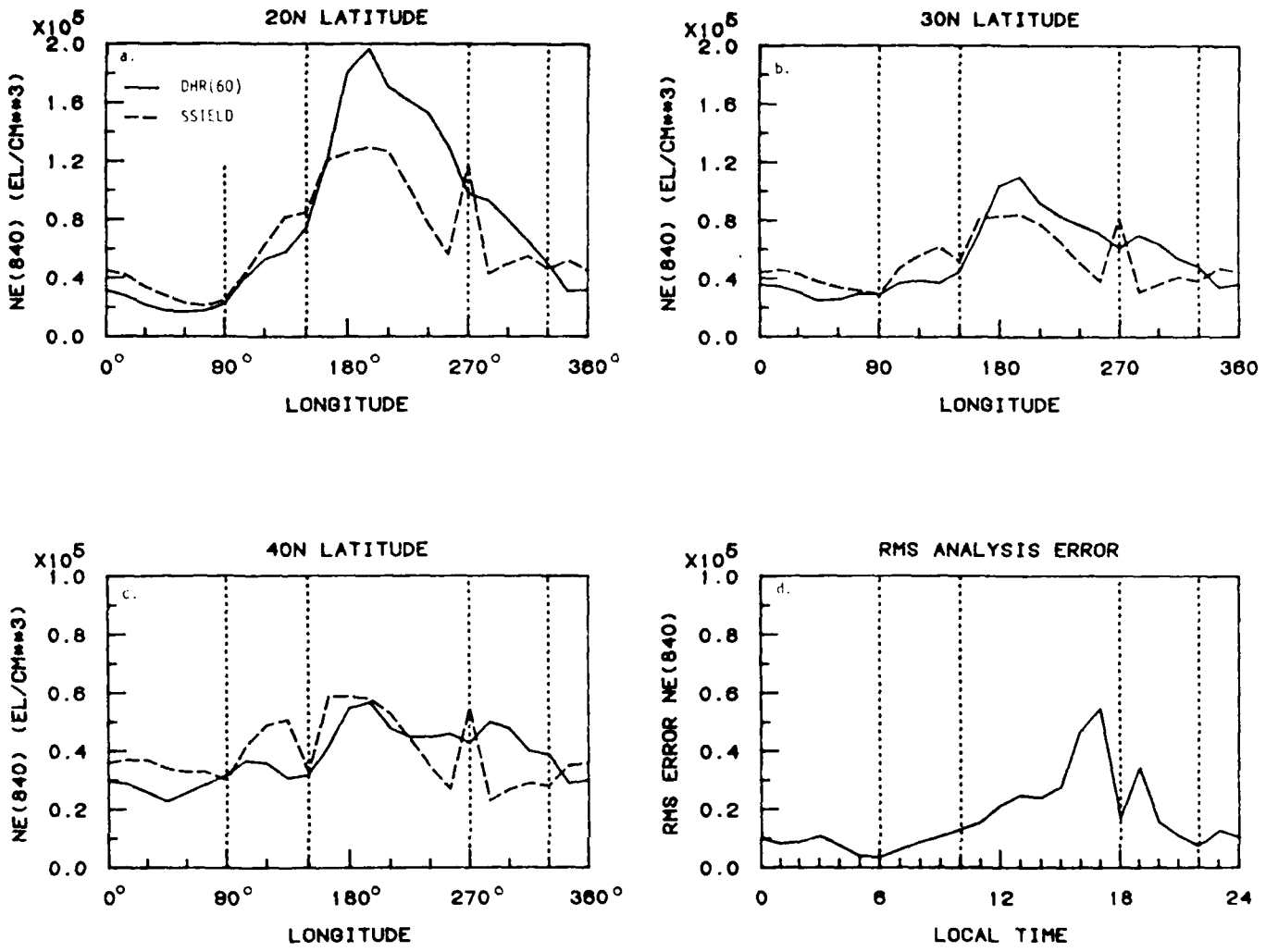

Figure 8. Representative results of the SSIELD assessment tests.

latitudes 00°-70° and a very large error at 80°. This same effect caused the increases instead of dips in the RMS percent error plot at 1000LT and 1800LT.)

This high-latitude problem is caused somewhere in the construction of the LT maps. Figures 9a-d show the variation of $N_e(840)$ with latitude at 0600, 1800, 1000, and 2200LT from the 00UT map of the DHR(60) two-satellite test. The solid lines are from the model, the dashed lines are results from the LT maps, and the dotted lines are from the final SSIELD output. The large increase at 80° latitudes shows up quite clearly in the 1000 and 1800LT maps. The problem at the equator also shows up in these plots, indicating that it, too, may be due to a problem in the LT map analysis.

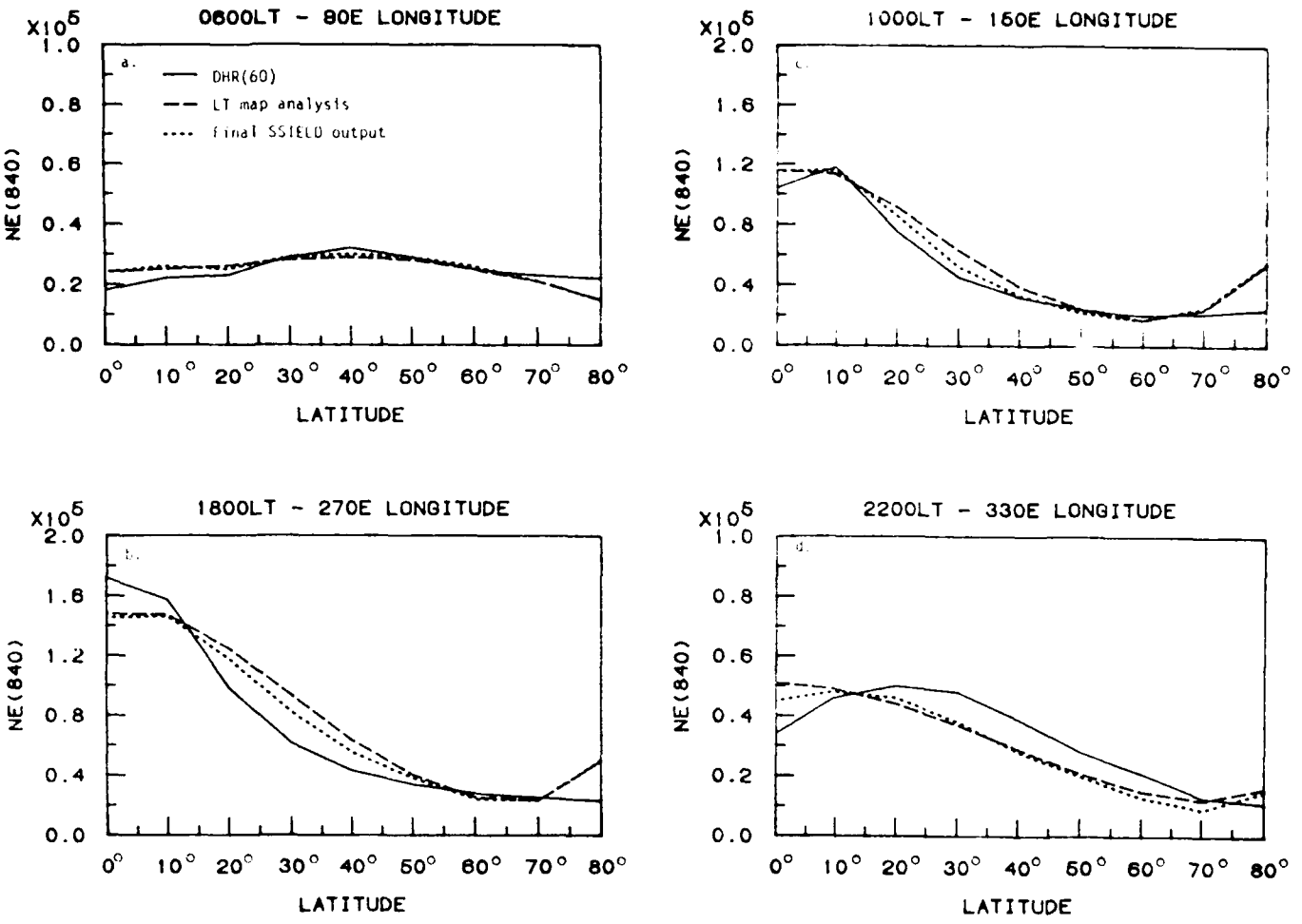

Figure 9. Latitudinal variation of $N_e(840)$ from the DHR(60) data, the LT map analysis output, and the final SSIELD analysis output.

In summary, the following problems and deficiencies were identified:

1. LT map construction.

a. The decimation scheme used to reduce the input data to 100 points per LT map effectively throws out over 60% of the available northern-hemisphere data.

b. Interpolation in time is not employed in using the spectral Bent model to "correct" data to the desired local time. (see 3b. below).

c. The assumptions made in constructing the covariance function that the field is homogeneous and isotropic may be unwarranted. In particular, studies have found that correlation distances of ionospheric density variations are different in the magnetic north-south and east-west directions[24].

d. The β-parameter estimation scheme failed to produce a solution in 9 of 16 test cases.

e. The LT maps fit the data poorly at the "edges" of the field, i.e., at high latitudes and near the equator.

2. Time interpolation.

a. The model used for interpolating can produce unrealistic variations in $N_e(840)$.

b. The interpolation scheme can produce very sharp discontinuities at times when data (from the LT maps) are available, particularly if the data values are far different from those calculated by the model used for interpolating.

c. If the LT map analysis fails to provide an $N_e(840)$ value for a particular grid point, a value of zero is generated for that grid point rather than some representative $N_e(840)$ value.

3. Spectral Bent model.

a. Fields of $N_e(840)$ produced by the model can be unrealistic, occassionally containing negative density values.

b. The model is discontinuous in time. A different set of coefficients are used for each of 24 local times with no interpolation for times not on the hour.

c. The model is valid only for a single, unstated, solar epoch. A new model would need to be implemented as the solar epoch, as indicated by the mean sunspot number, changes.

4. General

a. The program has no "memory" capability; i.e., the starting point of the analysis is always the internal model.

b. Expanding the program to provide other capabilities, such as including the southern hemisphere in the analysis, would be difficult.

c. The documentation provided requires additional work to meet AFGWC and DoD standards, and neither the program code nor the in-line documentation (comments) meets AFGWC standards.

The limitations and shortcomings of the current SSIELD program were discussed with Dr. Rich (AFGL/PHG) and Mr. Bussey (AFGWC/TSIS), and a consensus was reached that although the analysis methods used in SSIELD were theoretically sound, they were probably inappropriate for the current application and would be inadequate to the task even if the problems were corrected. It was decided, therefore, to redirect the near-term efforts under this contract to identifying and investigating alternative analysis techniques for producing gridded fields of SSIE $N_e(840)$ data.

Toward this end, informal discussions were held with Dr. Rich and Mr. Bussey to determine the requirements be met by the SSIELD program. A distillation of these discussions provided the following list of requirements and desired attributes:

1. The program must be documented and tested in accordance with DoD Standard 7935, dated 15 Feb 1983[25], and with the AFGWC software standards[26].

2. The program must be coded in ANSI Standard X3.9-1978, as implemented in the UNIVAC ASCII FORTRAN.

3. Any internal model of $N_e(840)$ used should be a continuous function of latitude, longitude, time, season (day-of-year), and sunspot number (solar epoch).

4. Ideally, any internal $N_e(840)$ model should be based on satellite observations. Provisions for updating this model should be included.

5. Data from the SSIE sensor should be fetched from a user-defined section of the Astrogeophysical Data Base (AGDB).

6. Provisions for future incorporation of TEC data, from either the AGDB or from a TEC data preprocessor, should be included.

7. The analysis algorithm should use all data available and be able to process data from both northern and southern hemispheres.

8. If no data are available for a particular program run, the analysis should default to the internal model.

9. The analysis should incorporate a "memory" capability; i.e., the analysis field from a previous run could be used as the starting point for the current run.

10. The final analysis field should not contain distinct features (bull's-eyes or ridges) at points where data are available.

11. The locations of the grid points for the output grids should be defined such that they may be easily changed.

Although this is not an officially approved statement of requirements, it provides a starting point for an investigation of alternative analysis methods for incorporation in program *SSIELD*.

4.2 Task 4: $N_e(840)$ Data Preprocessor Improvements

The starting point for this study was a general review of various analysis methods developed for use in other ionospheric applications, in particular, those developed in constructing the ITS78 model ionosphere[13,27], those used in AFGWC program UKFILE for updating the ITS78 coefficients[11], and the global analysis method used in the 4D model[7]. From this review, and the requirements listed in Section 4.1.3, the following general design was developed for an improved SSIELD program:

1. The core of the program would be a spectral model of $N_e(840)$ which would include continuous variability with location, time, season, and solar epoch. The format of this model would be similar to the ITS78 f_0F2 and M3000 spectral models[13].

2. Input SSIE $N_e(840)$ data would be used to modify the coefficients of this model in two stages:

a. All mid-latitude data would be used to adjust the model through derivation of an effective 10.7cm solar flux (F10) defined as the F10 value which, when used by the $N_e(840)$ model, minimizes the mean difference between the model and the observations. A similar method for adjusting the ITS78 f_0F2 coefficients has been used at AFGWC for several years[28].

b. All data would be used to modify the coefficients resulting from the effective F10 analysis, or from a previous analysis, using a spectral data assimilation method developed by Flattery[29] and used in the global analysis section of the 4D model[7].

3. The required UT grids would be generated from either the base $N_e(840)$ model, the results of the effective F10 analysis, the results of the global analysis, or from the results of some previous analysis, at the discretion of the user.

Investigation of this design would be accomplished in four phases:

1. Define the form of the spectral $N_e(840)$ model. This would include selection of coordinate system, functions to be used in the spectral expansion, truncation limits on the spectral expansion, and selection of an initial model of $N_e(840)$ on which to base the spectral model. The final step of this phase would be the generation of coefficients for the spectral $N_e(840)$ model.

2. Develop the effective F10 analysis technique. The starting point for this phase would be the AFGWC UKFILE program[28].

3. Develop the global assimilation technique. The starting point for this phase would be the global analysis section of the 4D model[7].

4. Test the full analysis program on both model and "real-world" inputs to determine how best to control the analysis so the occurance of spurious features at data points is reduced with minimum loss in analysis accuracy.

work has begun on phases one and two of this study.

4.2.1 $N_e(840)$ Spectral Model Definition

The first step in defining the spectral $N_e(840)$ model was to select coordinate systems in which to describe the model's variations in solar epoch, season, time-of-day, and location. It was decided to use the same coordinates as the ITS78 model[13] for solar epoch (F10 - the solar 10.7cm radio flux for season (DOY - the day-of-the-year), and for time-of-day (UT - universal time)), but to use a different system for location. In developing the ITS78 model, Jones *et al*[27] found that using a coordinate system based on the configuration of the earth's magnetic field improved the analysis. Their choice of location coordinates was the modified dip latitude and geographic longitude, the modified dip latitude being defined as

$$x = \tan^{-1}\left[\frac{I}{\sqrt{\cos\lambda}}\right]$$

where I is the magnetic dip angle and λ is the geographic latitude. This system was not selected for this application as it did not meet the following requirements:

1. The system should provide both magnetic latitude and longitude within the same conceptual framework, as well as a logical extension to the calculation of a magnetic local time.

2. The latitude coordinate should behave as dip latitude near the dip equator and as corrected geomagnetic (CG) latitude in the auroral and polar regions.

3. Both geographic-to-magnetic and magnetic-to-geographic transformations are needed, and should be computationally fast.

An extensive study of magnetic coordinates and their applicability to ionospheric mapping problems conducted under another project led to the development of F-layer apex coordinates[30], a modification of apex coordinates developed by Van Zandt *et al*[31]. Figure 10 is a contour map of F-layer apex latitude and logitude. The latitude spacing is 10°, and the longitude spacing is 90°. The horizontal and vertical dashed lines indicate the F-layer apex equator and zero meridian respectively. This system is defined similarly to CG coordinates, but with respect to the dip equator instead of the dipole equator. Thus, since the dip and dipole equators merge at large distances

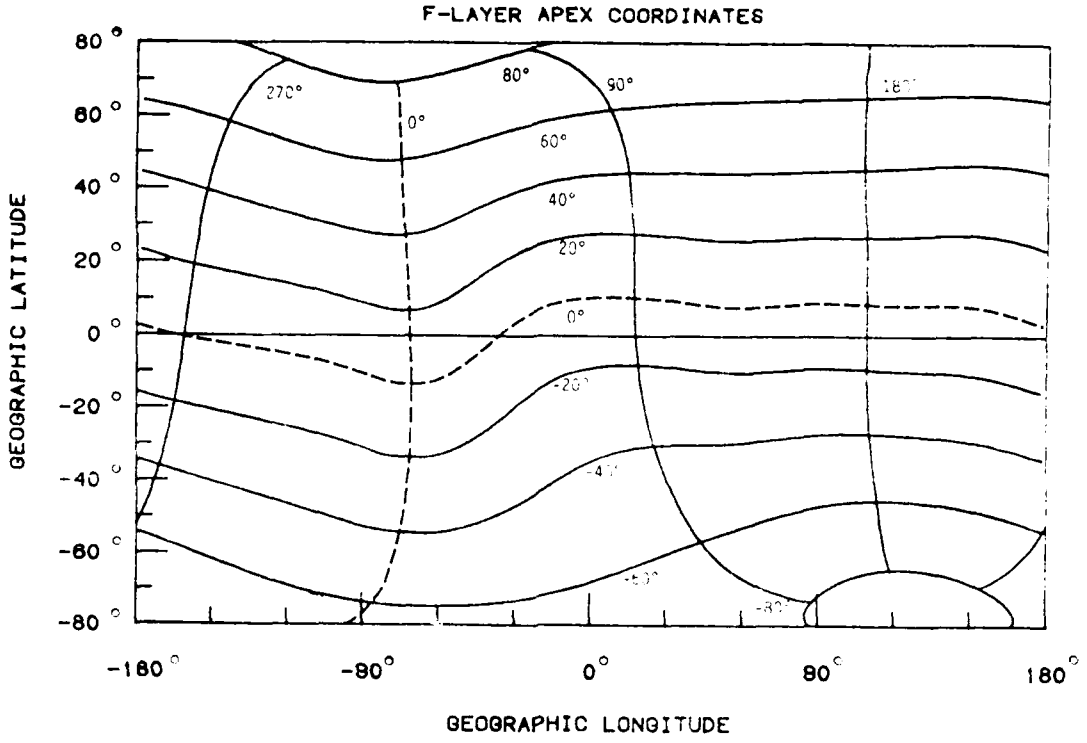

Figure 10. F-layer apex coordinates.

from the earth, F-layer apex latitude is similar to dip latitude near the common F-layer/dip equator and becomes identical to CG latitude at high latitudes. Algorithms to provide the required coordinate transforms were developed previously, as well as a look-up table for rapid calculation of F-layer apex coordinates from geographic coordinates[30]. Since this system meets all the stated requirements, and is readily available, it was decided to use F-layer apex coordinates for the location coordinate system.

The next step in the model definition was to select the expansion functions for each model variable. As with the selection of the coordinate systems, it was decided to use the functions selected for the ITS78 model for the solar epoch, season, and time-of-day variations. The solar epoch variation is expressed as a polynomial function in F10, the season variation as a trignometric series in DOY, and the time-of-day variation as a trignometric series in UT. For location functions, Jones *et al*[27] used a set of trignometric polynomials which are orthonormalized with respect to the locations of the input data for each analysis run. In the 40 model,

orthonormal associated Legendre functions, which are very similar to the *ad-hoc* set used in ITS78, are used to model the latitude-longitude variation. It was decided to use the associated Legendre functions for the following reasons:

1. The use of associated Legendre functions for spherical harmonic analysis, is a standard, well-documented analysis technique.

2. Associated Legendre functions were chosen for use in the 4D model to avoid singularity problems encountered in using the ITS78 functions in program UKFILE, the predecessor the 4D model[11].

3. The method to be used for the global assimilation, the 4D model global analysis method, is designed around a field expressed in associated Legendre functions. Thus, the amount of design work required is reduced if associated Legendre functions are used.

The final form selected for the $N_e(840)$ model is as follows:

$$N_e(\lambda,\phi,t,F,D;840) = \sum_{\ell=1}^{L}\sum_{m=1}^{M}\sum_{n=\frac{m}{2}}^{N} \gamma_\ell^{mn}(F,D)\; T_\ell(t)T_m(\phi)\; P_n^{m/2}(\sin\lambda) \qquad (9)$$

$$\gamma_\ell^{mn}(F,D) = \sum_{r=0}^{R}\left[\sum_{i=0}^{I} \alpha_{ri}^{mn} T_i(D)\right] F^r \qquad (10)$$

where λ and ϕ are F-layer apex latitude and longitude; t is UT; F is the 10.7cm solar flux; D is the day-of-the-year; $P_n^{m/2}(\sin\lambda)$ are the orthonormal associated Legendre functions of degree n and order $\frac{m}{2}$; and $T_\ell(t)$, $T_m(\phi)$, and $T_i(D)$ are orthonormal trignometric series given by

$$T_0(x) = \frac{1}{\sqrt{2\pi}}$$

$$T_{2j-1}(x) = \frac{1}{\sqrt{\pi}} \cos jx \quad ,$$

$$T_{2j}(x) = \frac{1}{\sqrt{\pi}} \sin jx \quad .$$

The next step is to select values for the five truncation limits in equations (9) and (10), L, M, N, R, and I.

The selection of the five truncation limits involves a rather complicated trade-off analysis between analysis accuracy and resolution requirements and operational size and run-time constraints. As no statement of operation constraints is available, the following targets were established based on informal discussions with AFGWC personnel: 1) run-time on the order of four minutes of CPU time or less on a UNIVAC 1100/82 for a 24-hour, two-satellite analysis, 2) executable program size under 60K, and 3) disk space requirements on the order of one position (~ 115K words) or less for all required data files. It was decided to approach the accuracy/resolution question by determining the maximum resolution afforded by the operational constraints. First, the truncation limits for equation (10) were set as the same as those used in the ITS78 model - I=8 and R=2, as was the value of the truncation limit for the UT expansion in equation (9) - L=13. This leaves the truncation limits on the associated Legendre function expansion, N, and M.

There are several truncation schemes available for a finite associated Legendre function series[32], such as the rhomboid scheme used in the 4D model, shown graphically in Figure 11. A modified triangular scheme, shown in Figure 12, was selected for the $N_e(840)$ model based on the following considerations:

1. The truncation scheme inherent in the ITS78 model, also shown in Figure 12, approximates a modified triangular truncation.

2. This scheme requires fewer functions than the 4D model scheme for the same maximum function degree for low longitudinal wave numbers.

3. This scheme acts as a filter to smooth out features which are small in both latitudinal and longitudinal extent.

The limits used in the truncation, M_p=10* and N=20 at m_p=0*, were selected to

---

*The truncation limit, M_p, and index, m_p, used in this discussion are related to M and m in equation (9) by

$$M_p=\frac{1}{2}(M-1)$$

$$m_p=\text{Integer}\left(\frac{1}{2}m\right).$$

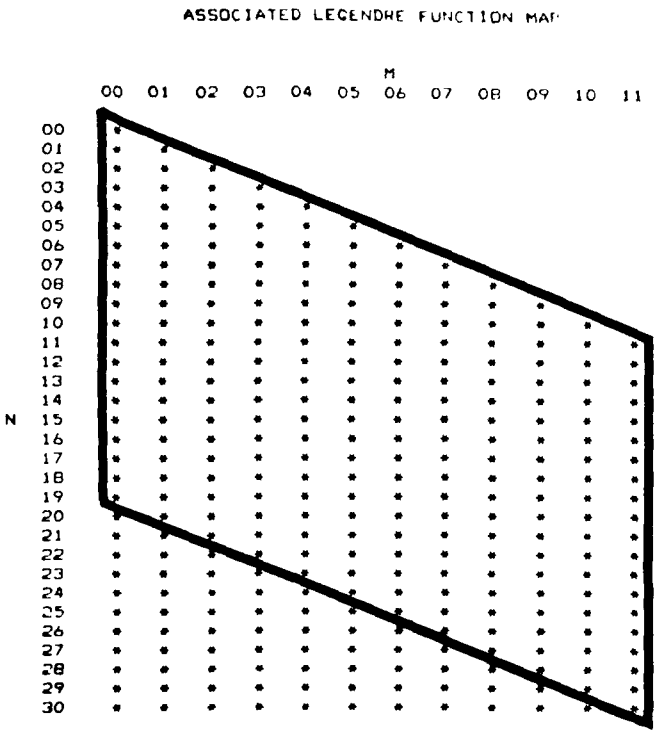

Figure 11. The rhomboid truncation scheme for an associated Legendre function series used in the 4D model.

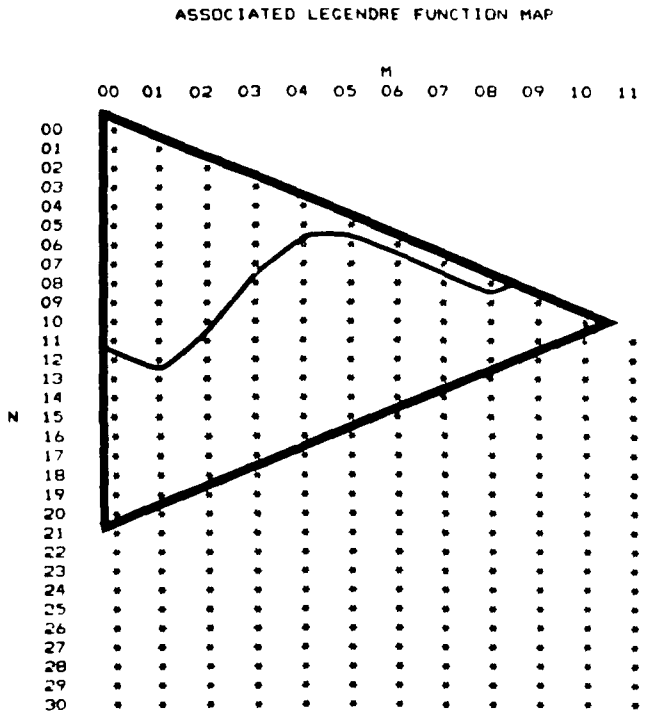

Figure 12. The modified triangle truncation scheme (heavy line) chosen for the $N_e(840)$ model and the inherent truncation employed in the ITS78 model (fine line).

match at least the value for N at m_p=0 used in the 4D model, N=19. The limits in equation (9) for this truncation are M=21 and N=20 - $\frac{m}{2}$.

A preliminary design for the data file to be used by this program was developed to estimate the disk space it would require. Included in the file would be the F-layer apex-coordinate transformation table (8190 words, 293 28-word sectors*), the coefficients for the spectral $N_e(840)$ model (one sector per time-location coefficient, 2873 sectors total), five sets of coefficients from previous analyses (2873 words, 103 sectors), and six file-control sectors, for a total of 3687 sectors. This is roughly 103K words, well within the target of 115K.

The final step in defining the spectral $N_e(840)$ model, prior to generating the model coefficients, was to select a model of $N_e(840)$ from which to generate the coefficients. Since this analysis program is being developed for use at AFGWC, it was decided to use the DHR profile model in conjunction with the ITS78 f_oF2 and M3000 models, at least for initial design and testing. It is planned to obtain a copy of the Bent profile model[23] and construct a set of spectral model coefficients for it as well, for comparison testing with actual SSIE data. The software used to calculate the spectral model coefficients and all routines which use them will be designed such that they are completely independent of the $N_e(840)$ model used in generating the coefficients.

The coefficients of the spectral $N_e(840)$ model are calculated by a least-squares fit of the model functions to fields generated by the ITS78-DHR (or ITS78-Bent) models. In order to reduce the dynamic range of the $N_e(840)$ fields, the probable source of the negative $N_e(840)$ values in the SSIELD model, the density values are converted to the equivalent plasma frequency, $f_p(840)$, prior to performing the least-squares fits. The ITS78-DHR model is used to build 10° latitude by 15° longitude grids in F-layer apex coordinates covering the range -80° to +80° latitude for each UT hour (00-23), for each month of the year, for F10 values of 70, 120, 170, and 220. Each of the 48 sets of time-location grids is reduced to 48 sets of 2873 coefficients using least-squares fits to the time, $T_t(t)$, and location, $T_m(\phi)P_n(\sin\lambda)$, functions in equation (9). These are further reduced to 12 sets of 8619

*The file size is defined in terms of 28 word sectors as the UNIVAC 1100/82 computer uses sector-addressable I/O to disk mass storage. Disk space is allocated by track (64 sectors) or position (64 tracks).

coefficients by a least-squares fit in F10, and finally to a set of 77,571 coefficients by a fit in season.

A complete coefficient set has not yet been generated, although sub-sets have been generated to test all three fitting procedures. Figures 13 and 14 show sample results of the time-location fits. The upper plot in each figure is the ITS78-DHR $N_e(840)$ field, and the lower plot is from equation (9) using the coefficients from the time-location fit. These plots are in F-layer apex coordinates with a geographic latitude-longitude grid overlay. Figures 15 and 16 are examples of the results of the F10 fits, showing sample latitude and UT variations, and Figure 17 shows the seasonal fit to the first time-location coefficient for F10 = 70. All of the fits are within acceptable limits. A complete set of coefficients modeling the F10 and time-location variations for the month of May have been generated for initial testing of the effective F10 analysis.

4.2.2 Effective F10 Analysis

The first stage in the new analysis scheme consists of adjusting the value of F10 used in the coefficient equation

$$\gamma_{\ell}^{mn} = \sum_{r=0}^{2} \beta_{r}^{\ell mn} F10^{r}$$

where

$$\beta_{r}^{\ell mn} = \sum_{i=1}^{9} \alpha_{ri}^{\ell mn} T_i(D) ,$$

until the average difference between all mid-latitude $N_e(840)$ data and the values calculated using equation (9) is minimized. This value of F10 is denoted the effective F10 value for the analysis and is conceptually equivalent to the effective sunspot number (SSN) calculated in AFGWC program UKFILE by fitting observed f_0F2 values with the ITS78 model[28]. An initial test of this technique, using the binary search algorithm from UKFILE, was run using data along a simulated dawn-dusk DMSP orbit extracted from a time-location $N_e(840)$ grid set calculated for F10 = 170. Given an initial F10 value of 120, the analysis calculated an effective F10 of 170.2 in 6 iterations. Although the accuracy shown in this test was more than acceptable, it is hoped that using a more sophisticated search algorithm could

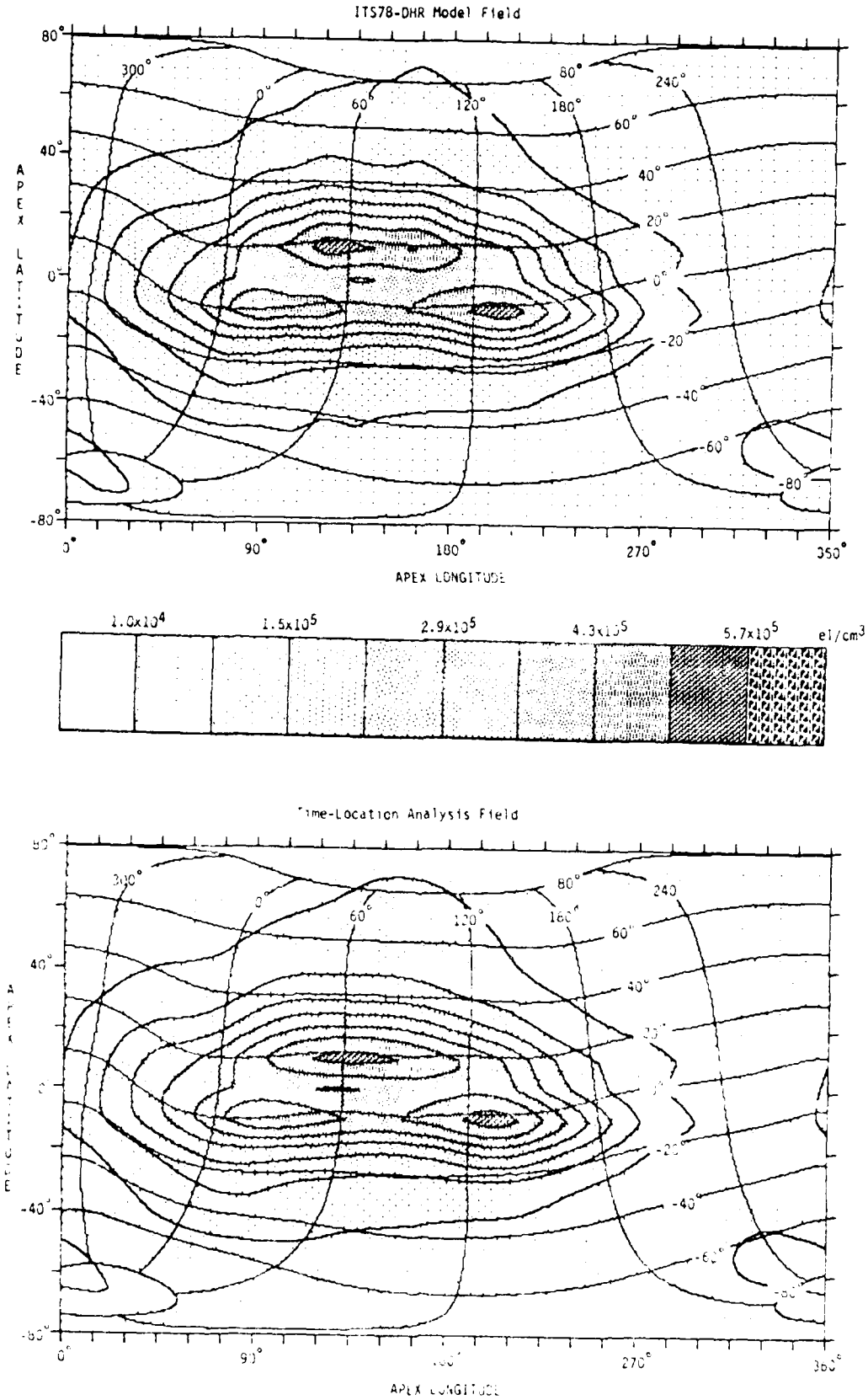

Figure 13. Sample results from the time-location analysis for 15 May, 1200 UT, F10=170.

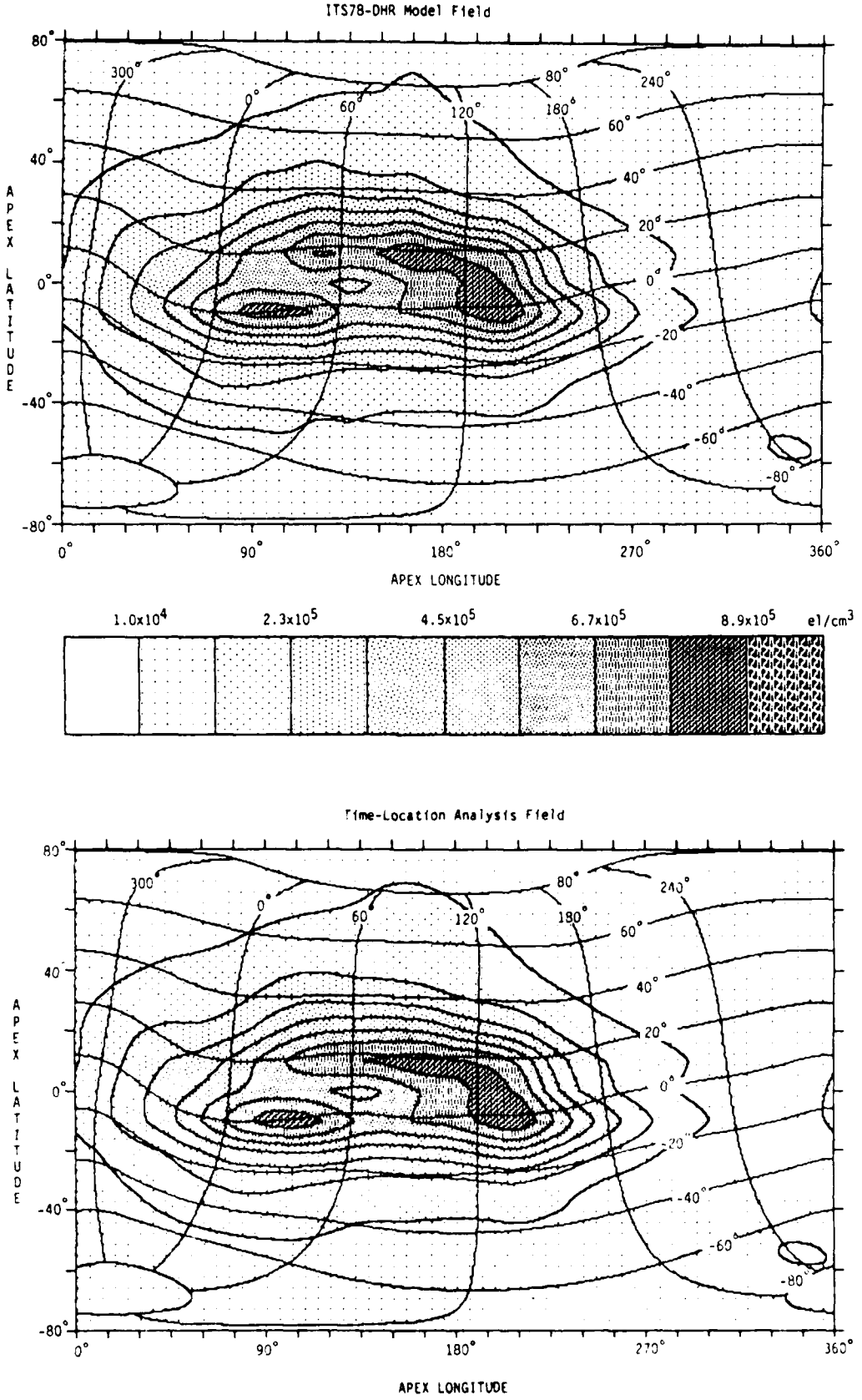

Figure 14. Same as Figure 13 for F10=220.

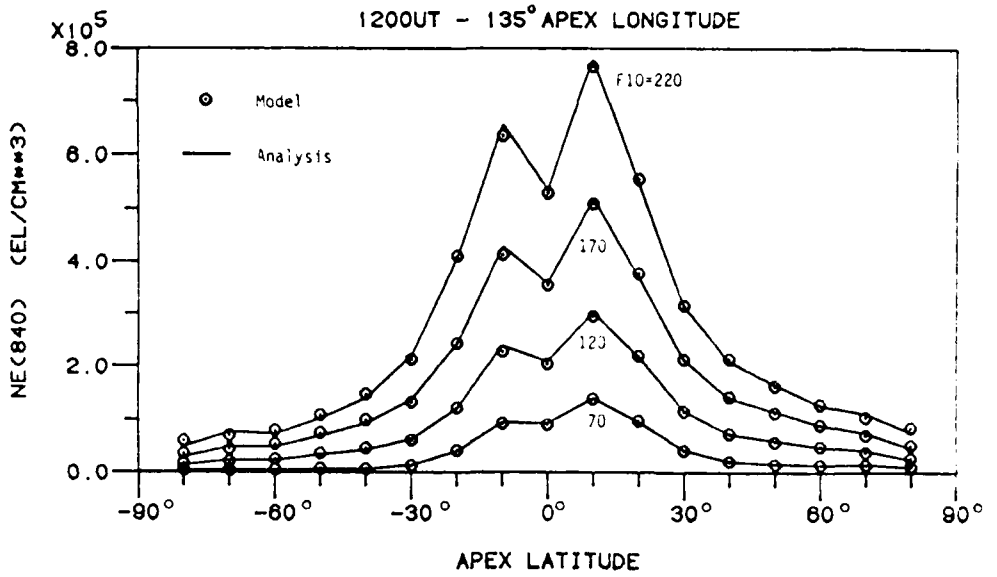

Figure 15. Sample results from the F10 analysis - latitudinal variation.

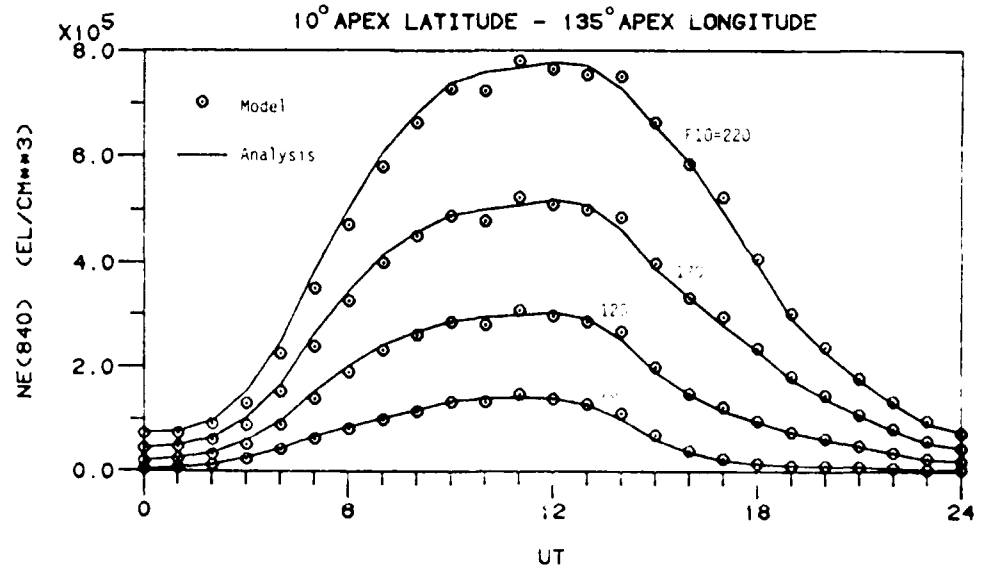

Figure 16. Same as Figure 15 - UT variation.

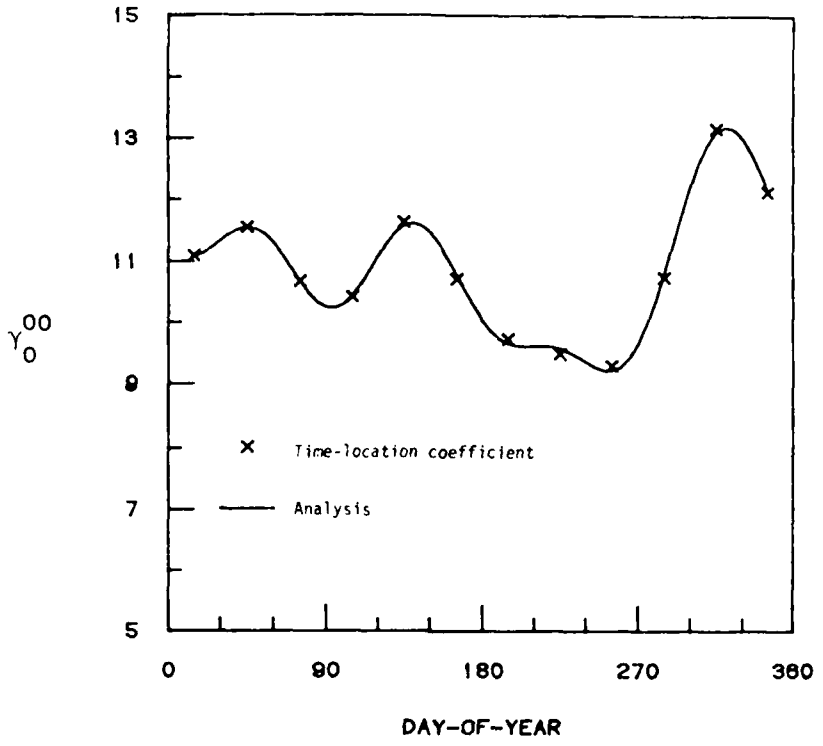

Figure 17. Sample results from the season analysis. Shown is a plot of the γ_0^{00} coefficient (see Equation 10) from each month of the time-location analysis for F10-70 (crosses) and the results of the season analysis for this coefficient.

possibly achieve similar accuracy in fewer iterations. An evaluation of other search algorithms is the next step in the current study. When this is completed, work will begin on the global analysis method.

4.3 Task 5: Combined TEC and $N_e(840)$ Data Preprocessor

Other than informal discussions with personnel from AFGWC/TSIS (Mr. Bob Bussey) and AFGL/LIS (Mr. Jack Klobuchar), little has been done on this Task pending resolution of the problems with the current $N_e(840)$ preprocessor and formal tasking within AFGWC for Mr. Bussey to work on improvements to the TEC preprocessor. One possible method for combining the two data types in a single analysis would be to convert TEC to an effective $N_e(840)$ and process it with the SSIE $N_e(840)$ data[2]. This will be investigated when the work described in Section 4.2 has been completed.

5. 4D MODEL IMPROVEMENTS STUDY

The two tasks which make up this study, Tasks 1 and 3, were both completed during this project year, although Task 3 was modified slightly as a result of the IRI79 model study discussed earlier.

5.1 Task 1: 4D Model Global Analysis

The 4D model, as originally configured, produced analyses of the northern hemisphere only in order to reduce both program size and model run-time. This is done by assuming that the southern hemisphere is a mirror-image of the northern hemisphere, thus forcing the coefficients of all odd associated Legendre functions, P_n^m, to be zero. Thus, only the even P_n^m functions and their coefficients need be processed, reducing the total number of coefficients by a factor of two, as well as the run time of the global analysis section of the 4D model. Unfortunately, the result was that half of the data collected by the SSIE sensor, i.e. all southern hemisphere data, were not usable by the 4D model. The objective of Task 1 was to determine what modifications were required to configure the 4D model for a true global analysis.

As it turned out, only a few modifications to the 4D model are required to allow the model to be configured for either global or hemispheric analysis. These were:

1. Insure that the routine used to calculate the associated Legendre functions calculates both even and odd functions.

2. Set up a parameter which specifies the model configuration.

3. Set up parameters for all array dimensions, array sizes, and DO-LOOP range variables to be functions of the configuration parameter.

4. Change all code in the model which limits the analysis to the northern hemisphere to be configuration dependent.

5. Document the procedures for configuring the 4D model in full global analysis mode.

These changes were implemented in the 4D model as part of a separate contract, and the configuration change procedures were included in the documentation provided as part of that project[8].

These modifications will improve the utilization of southern hemisphere SSIE observations, but it is doubtful that this mode will be operationally useable for real-time applications, as it doubles both the number of coefficients required for analysis and the model run-time over a single-hemisphere analysis.

5.2 Task 3: Model-based 4D Height Functions

The 4D model uses a set of empirically-derived orthonormal functions to describe the height variation of the ionospheric electron density[7]. The original function set was derived from a set of electron density profiles collected by the Millstone Hill incoherent scatter radar, extrapolated downward to 95km and upward to 2000km using the DHR model[18]. Limited studies of the 4D model during the late 1970's[19,20] showed that the Millstone Hill function set could not adequately match observed electron density profiles at other than mid-latitudes, and for moderate to high sunspot numbers at all latitudes. This problem was magnified by the differences in shape between profiles built by the DHR model from input data and those produced by the Millstone Hill functions.

The optimal set of data from which to construct a more representative height function set would be a collection of incoherent radar soundings covering the height range 100-2000km from equatorial, middle, auroral, and polar latitudes at various longitudes for at least one solar cycle. As the collection of such a data set is unfeasible, it was proposed to use the IRI79 model to construct such a data set from which height functions could be constructed. The reasons for choosing the IRI79 model were twofold:

1. The IRI79 model was constructed from as extensive a data base as possible to cover most ionospheric regimes, and

2. It was proposed to incorporate the IRI79 profile parametrization into the 4D model (Task 2 of this project). Thus, there would be no conflicts between the internal profile model and the height functions.

The results of the IRI79 study conducted in Task 2, and the decision based on that study not to use the IRI79 parametrization within the 4D model, have led to a modification of this task. Since the 4D will continue to use the DHR profile model, it was decided to construct height function sets from a collection of profiles built from the DHR model. While this is a somewhat less than optimal data set, this will at least alleviate problems caused by conflicts between the internal profile model and the height functions.

Three sets of DHR model profiles were generated and height function sets calculated from them during visits to AFGWC. All three sets consisted of a collection of 5184 profiles generated for a 10° latitude by 15° longitude by 1^{h} local time, northern-hemisphere grid covering a height range of 95-2000km. Set 1 included profiles generated for four solar epochs (sunspot numbers 10, 50, 90, and 130) and two seasons (15 June and 15 December), set 2 included profiles generated for two solar epochs (sunspot numbers 20 and 120) and four seasons (15 March, 15 June, 15 September, and 15 December), and set 3 was generated for a single sunspot number (56) and date (20 September). Figures 18a-18d show the four height functions extracted from these three sets, as well as the original Millstone Hill functions. Only the lower 1000 kilometers are plotted, as all four functions shown decay exponentially toward zero in the 1000-2000km height range.

These new height function sets and the software required to generate additional sets were provided to AFGWC, and the procedures for height function set generation were formally documented as part of a separate contract[8]. Additional sets for other solar epoch/season combinations will be generated during the next project year, as well as for the new height profile model being developed under Task 6, should it prove to be a viable replacement for the DHR model.

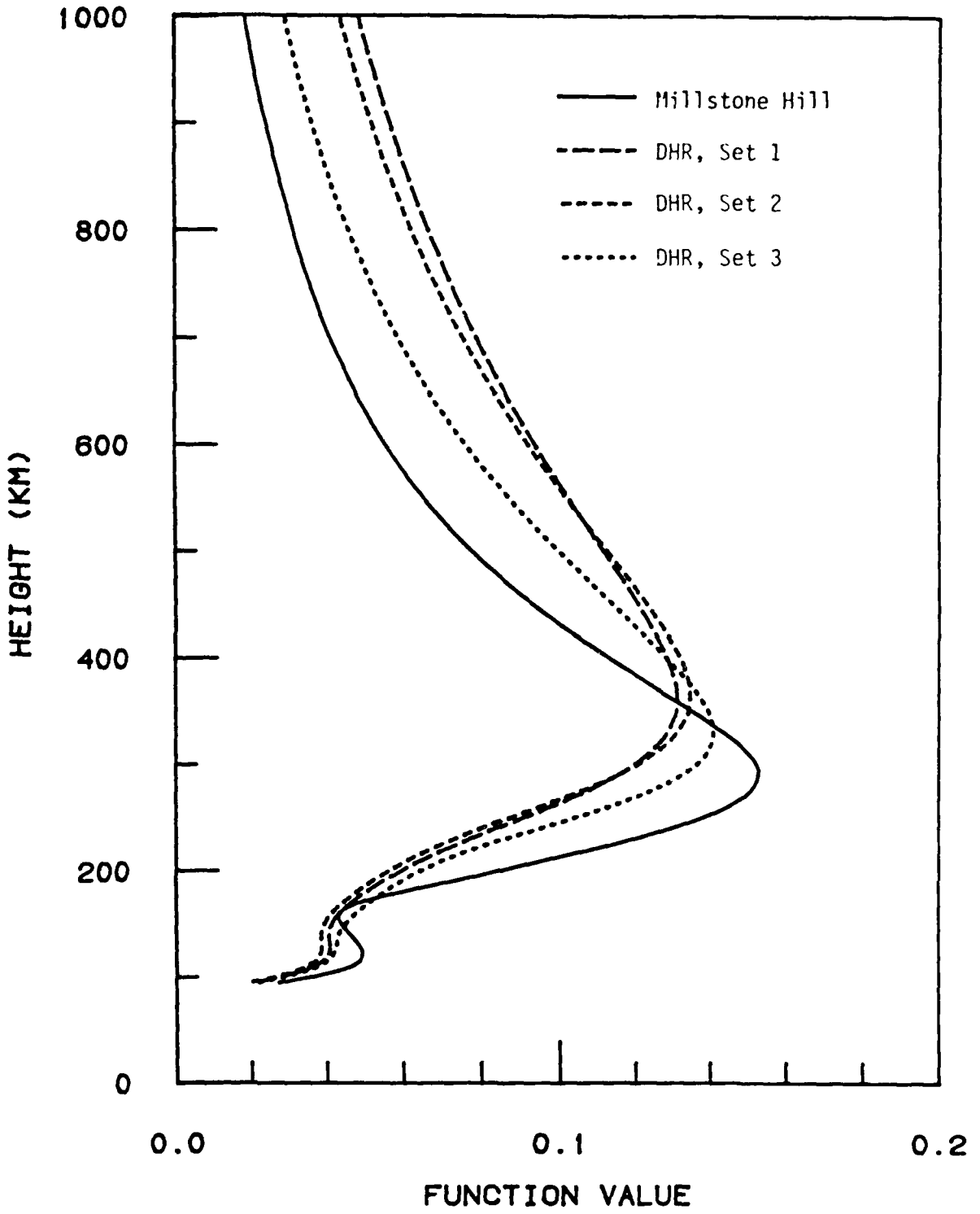

Figure 18a. First 4D height functions derived from Millstone Hill and three DHR model profile data sets.

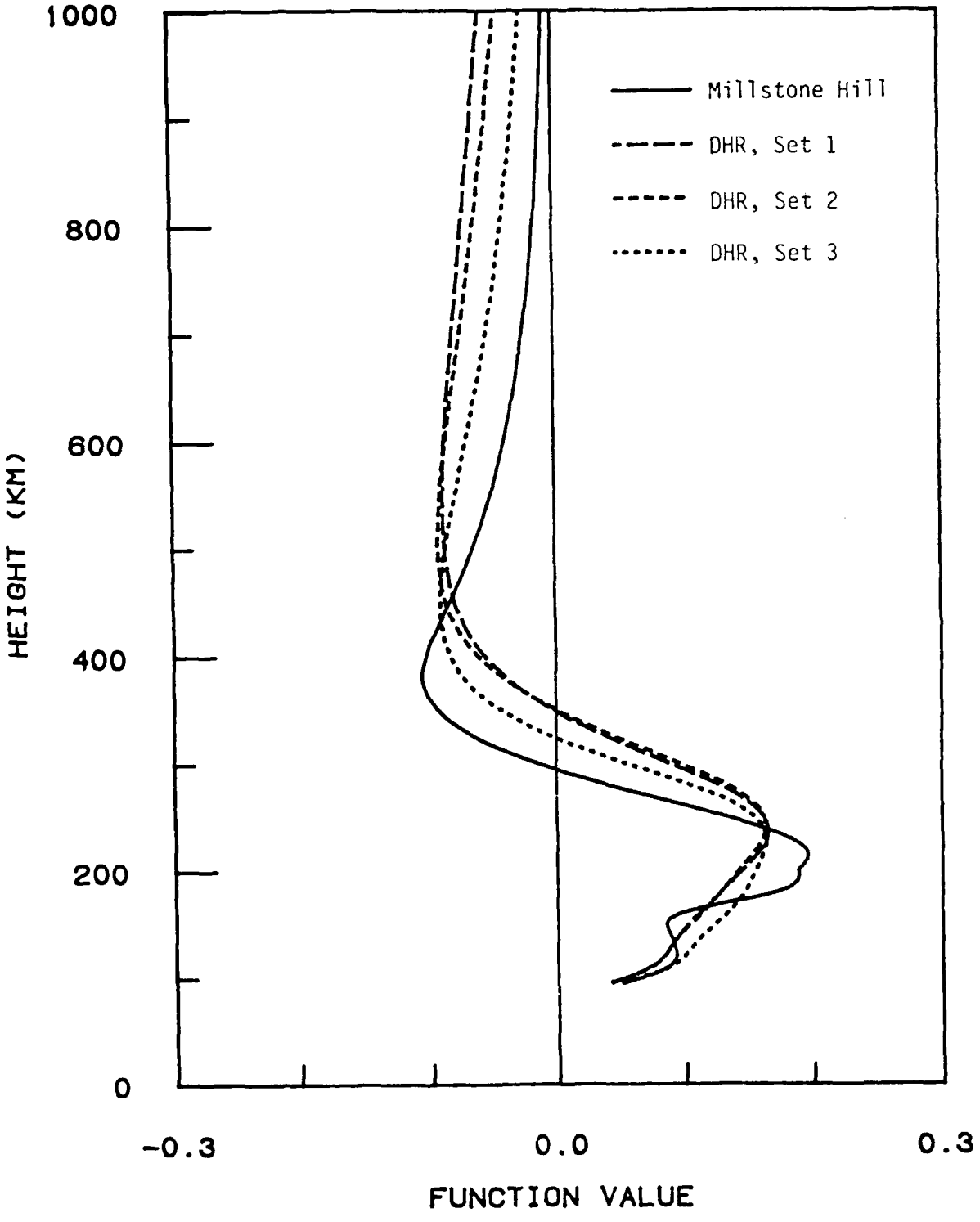

Figure 18b. Second 4D height functions as in Figure 18a.

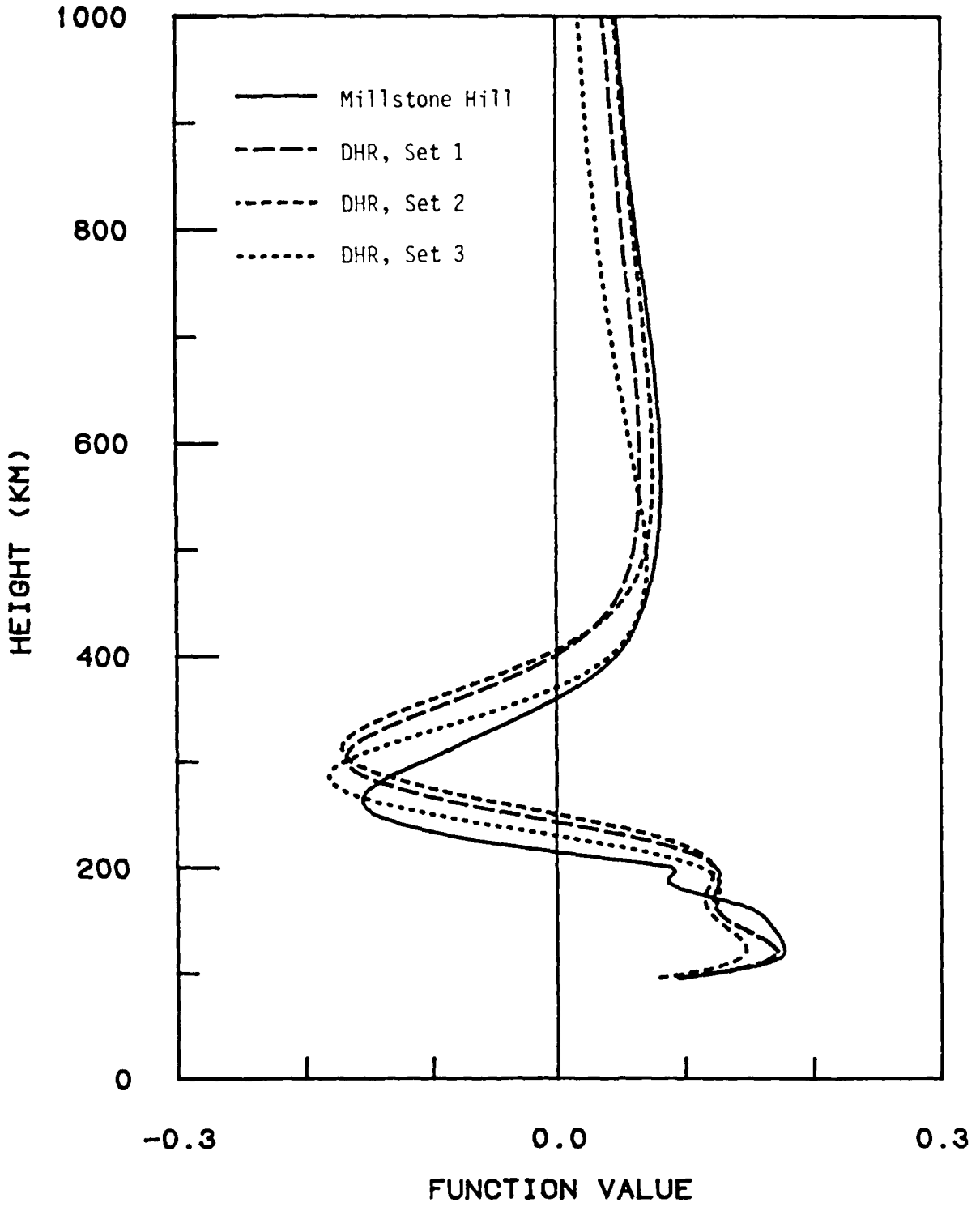

Figure 18c. Third 4D height functions as in Figure 18a.

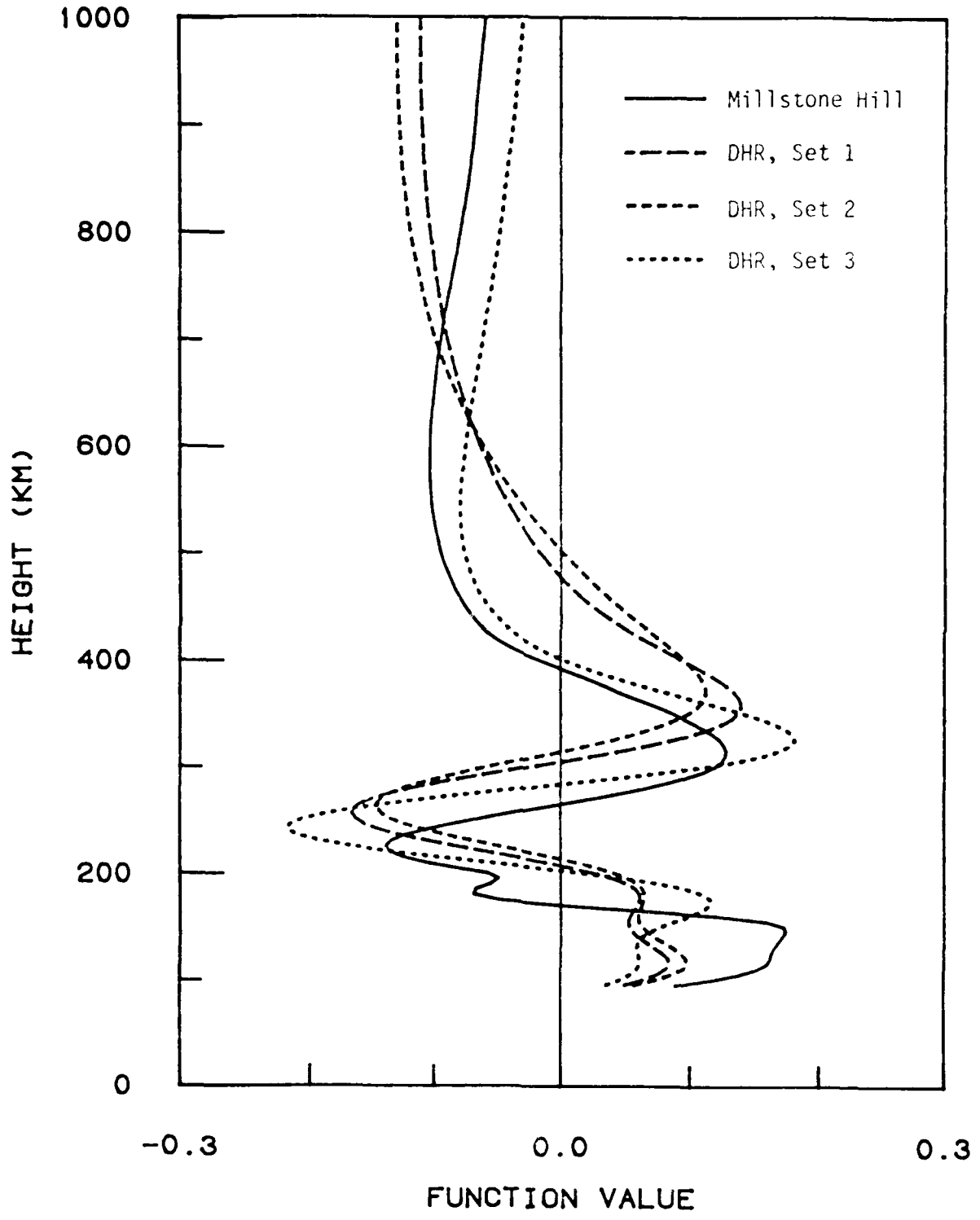

Figure 18d. Fourth 4D height functions as in Figure 18a.

6. CONCLUSION

Work on this project has progressed satisfactorily during its first year. The only difficulties encountered were the unexpected inadequacy of the IRI79 topside parametrization and the problems described in Section 4.1 with the current SSIE $N_e(840)$ preprocessor, program SSIELD. The main efforts planned for the second project-year are continuation of work on Task 4 to improve the $N_e(840)$ preprocessor, and on Task 6, to investigate alternative topside parametrizations for the 4D profile model. At the completion of Task 4, work will begin on Task 5, an investigation of methods for combining TEC and $N_e(840)$ data into a single analysis.

REFERENCES

1. Secan, J.A., DMSP SSIE Topside Data Interface System, System Documentation, Report No. PD-NW-82-275R, Physical Dynamics, Inc., Bellevue, WA 98009, September 1982.

2. Smiddy, M., Sagalyn, R.C., Sullivan, W.P., Wildman, P.J.L., Anderson, P., and Rich, F., The Topside Ionosphere Plasma Monitor (SSIE) for the Block 5D/Flight 2 Satellite, AFGL-TR-78-0071, ADA058503, Air Force Geophysics Laboratory, Hanscom AFB, MA 01731, March 1978.

3. Rich, F., Smiddy, M., Sagalyn, R.C., Burke, W.J., Anderson, P., Bredesen, S., and Sullivan, W.P., In-Flight Characteristics of the Topside Ionospheric Monitor (SSIE) on the DMSP Satellite Flight 2 and Flight 4, AFGL-TR-80-0152, ADA088879, Air Force Geophysics Laboratory, Hanscom AFB, MA 01731, April 1980.

4. Air Force Global Weather Central Data Format Handbook, Air Force Global Weather Central, Offutt AFB, Ne 68113, September 1983 (available through Hq Air Weather Service/DNTS, Scott AFB, IL 62225).

5. Siong-Huat, C., DMSP SSIE Uniform Grid Generator (Program SSIELD), System Documentation, Bedford Research Associates, Bedford, MA 01730, June 1983.

6. Secan, J.A. and Tascione, T.F., "The 4D Ionospheric Objective Analysis Model," in Proceedings of the 1984 Symposium on the Effect of the Ionosphere on C3I Systems, To be published, 1984.

7. Secan, J.A., 4D Ionospheric Analysis Model, System Documentation, Report No. PD-NW-83-297R-1, Physical Dynamics, Inc., Bellevue, WA 98009, December 1983.

8. Lincoln, J.V. and Conkright, R.O., International Reference Ionosphere -IRI79, Report UAG-82, World Data Center for Solar-Terrestrial Physics, Boulder, CO 80303, November 1981.

9. Damon, T.D. and Hartranft, F.R., Ionospheric Electron Density Profile Model, Technical Memorandum 70-3, Aerospace Environmental Support Center, Ent AFB, CO, July 1970 (available from the USAF Air Weather Service Technical Library, Scott AFB, IL 62225).

10. Flattery, T.W. and Ramsay, A.C., "Derivation of Total Electron Content for Real Time Applications," Effect of the Ionosphere on Space Systems and Communications, Naval Research Laboratory, Washington, DC, pp. 336-344, 1975.

11. Watt, T.M., "Ion Distribution and Temperature in the Topside Ionosphere from the Alouette Satellite," J. Geophys. Res., 70, pp. 5849-5859, December 1965.

12. Jones, W.B. and Obitts, D.L., Global Representation of Annual and Solar Cycle Variation of foF2 Monthly Median 1954-1958, OT/ITS Research Report 3, Institute for Telecommunication Sciences, Boulder, CO, October 1970.

13. McNamara, L.F. and Wilkinson, P.J., "Prediction of Total Electron Content Using the International Reference Ionosphere," J. Atmos. Terr. Phys., 45, pp. 169-174, 1983.

14. Titheridge, J.E., "Ion Transition Heights from Topside Electron Density Profiles," Planet. Space Sci., 24, pp. 229-245, 1976.

15. Kutiev, I., Heelis, R.A., and Sanatani, S., "The Behavior of the O^+-H^+ Transition Level at Solar Maximum," J. Geophys. Res., 85, pp. 2366-2372, May 1980.

16. Titheridge, J.E., "Plasmapause Effects in the Top Side Ionosphere," J. Geophys. Res., 81, pp. 3227-3233, July 1976.

17. Tascione, T.F., Flattery, T.W., Patterson, V.G., Secan, J.A., and Taylor, J.W., "Ionospheric Modeling at Air Force Global Weather Central," Solar-Terrestrial Predictions Proceedings, Volume I, Space Environment Laboratory, Boulder, CO, pp. 367-377, August 1979.

18. Tascione, T.F. and Secan, J.A., 4-D Technical Description, 4D Model Documentation, Air Force Global Weather Central, Offutt AFB, NE, 1978 (available through Hq Air Weather Service/DNTS, Scott AFB, Il 62225).

19. Tascione, T.F., 4-D Technical Description/2, 4D Model Documentation, Air Force Global Weather Central, Offutt AFB, NE, 1979 (available through Hq Air Weather SErvice/DNTS, Scott AFB, Il 62225).

20. Thompson, R.L. and Secan, J.A., "Geophysical Forecasting at AFGWC," Solar-Terrestrial Predictions Proceedings, Volume I, Space Environment Laboratory, Boulder, CO, pp. 350-366, August 1979.

21. Ripley, B.D., Spatial Statistics, John Wiley & Sons, New York, NY, pp. 44-75, 1981.

22. Llewellyn, S.K. and Bent, R., Documentation and Description of BENT Ionospheric Model, AFCRL-TR-73-0657, AD772733, Air Force Geophysics Laboratory, Hanscom AFB, MA, 1973.

23. Rush, C.M. and Edwards, W.R., "An Automated Technique for Representing the Hourly Behavior of the Ionosphere," Radio Science, 11, pp. 931-937, November 1976.

24. Automated Data Systems (ADS) Documentation, Department of Defense Standard 7935, February 1983.

25. AFGWC Software Standards, Air Force Global Weather Central, Offutt AFB, NE, March 1983 (available through Hq Air Weather Service/DNTS, Scott AFB, Il 62225).

26. Jones, W.B., Graham, R.P., and Leftin, M., Advances in Ionospheric Mapping by Numerical Methods, ESSA Technical Report ERL 107 - ITS 75, Institute for Telecommunication Sciences, Boulder, CO, May 1969.

27. von Flotow, C.S., "Ionospheric Forecasting at Air Force Global Weather Central," Effect of the Ionosphere on Spa and Terrestrial Systems, Naval Research Laboratory, Washington, DC, pp. 385-392, 1978.

28. Flattery, T.W., "Spectral Models for Global Analysis and Forecasting," Automated Weather Support, AWS-TR-242, Air Weather Service, Scott AFB, IL, pp.42-54, April 1971 (available from the USAF Air Weather Service Technical Library, Scott AFB, Il 62225).

29. Secan, J.A., Definition of Procedures for Gridding the WBMOD Ionospheric Scintillation Model, PD-NW-83-292R, Physical Dynamics, Inc., Bellevue, WA 98009, April 1983.

30. Van Zandt, T.E., Clark, W.L. and Warnick, J.M., "Magnetic Apex Coordinates: A Magnetic Coordinate System for the Ionospheric F2 Layer," J. Geophys. Res., 77, pp. 2406-2411, May 1972.

31. Machenhauer, B., "The Spectral Method," Numerical Methods Used in Atmospheric Models, Vol II, World Meterorology Organization, Geneva, Switzerland, pp. 121-275, 1979.

END

2-87

DTIC